Journal of Volcanology and Geothermal Research 177 (2008) 549–568

Contents lists available at ScienceDirect

Journal of Volcanology and Geothermal Research

journal homepage: www.elsevier.com/locate/jvolgeores

Englacial tephrostratigraphy of Erebus volcano, Antarctica

C.J. Harpel [a,b,*], P.R. Kyle [a], N.W. Dunbar [c]

[a] Department of Earth and Environmental Science, New Mexico Institute of Mining and Technology, Socorro, NM, 87801, USA
[b] Department of Geosciences, 104 Wilkinson Hall, Oregon State University, Corvallis, OR, 97331-5506, USA
[c] New Mexico Bureau of Geology and Mineral Resources, New Mexico Institute of Mining and Technology, Socorro, NM, 87801, USA

ARTICLE INFO

Article history:
Received 15 June 2006
Accepted 2 June 2008
Available online 7 June 2008

Keywords:
Erebus volcano
tephrostratigraphy
tephra
geochemistry
eruptive history
Antarctica

ABSTRACT

A tephrostratigraphy for Erebus volcano is presented, including tephra composition, stratigraphy, and eruption mechanism. Tephra from Erebus were collected from glacial ice and firn. Scanning electron microscope images of the ash morphologies help determine their eruption mechanisms The tephra resulted mainly from phreatomagmatic eruptions with fewer from Strombolian eruptions. Tephra having mixed phreatomagmatic–Strombolian origins are common. Two tephra deposited on the East Antarctic ice sheet, ~200 km from Erebus, resulted from Plinian and phreatomagmatic eruptions. Glass droplets in some tephra indicate that these shards were produced in both phreatomagmatic and Strombolian eruptions. A budding ash morphology results from small spheres quenched during the process of hydrodynamically splitting off from a parent melt globule. Clustered and rare single xenocrystic analcime crystals, undifferentiated zeolites, and clay are likely accidental clasts entrained from a hydrothermal system present prior to eruption. The phonolite compositions of glass shards confirm Erebus volcano as the eruptive source. The glasses show subtle trends in composition, which correlate with stratigraphic position. Trace element analyses of bulk tephra samples show slight differences that reflect varying feldspar contents.

© 2008 Elsevier B.V. All rights reserved.

1. Introduction

Tephra contained in glacial ice on the flanks of and adjacent to Mount Erebus and at several locations along the Transantarctic Mountains provide insight into the explosive eruptive history of Erebus volcano (Fig. 1). Chemical compositions and statistical correlation help determine Erebus to be the source for all of the tephra. As the tephra are preserved in stratigraphic order we are also able to examine changes in the magma composition with time. The morphology of ash particles from the tephra allows an understanding of the eruptive dynamics of the eruptions and provides insight into the eruptive history of Erebus volcano.

An extensive tephrostratigraphy for Antarctica has been established using tephra layers found in ice cores, exposed blue ice areas, and sedimentary deposits throughout the continent (Smellie, 1999). The tephrostratigraphy is somewhat limited because many tephra are located far from their volcanic sources and provide only a distal record for large eruptions. In many cases the source volcanoes for the tephra deposits have not been identified, as they are located on other continents or oceanic islands at great distances from Antarctica. Detailed explosive eruptive histories and tephrostratigraphies of individual volcanoes are very limited for several reasons. Due to their isolation, many volcanoes in Antarctica are understood only at a reconnaissance level and completely lack any geochronologic framework (LeMasurier and Thompson, 1990). The thick sequences of proximal pyroclastic deposits preserved at most volcanoes are typically lacking because friable deposits are quickly eroded by the harsh weather conditions and extreme glaciation in Antarctica. The ability for snow to preserve even the smallest tephra layers is an important aspect of tephrostratigraphic work in Antarctica. The snow transforms to glacial ice as it is buried and preserves tephra deposits such as those on the slopes of Erebus volcano.

Tephra were sampled from the Barne Glacier on the western flank of Erebus (Fig. 1) at 3 sites referred to as Lower Barne (LB), Middle Barne (MB), and Upper Barne (UB). The 3 sites represent a stratigraphic order, with LB being the oldest and UB the youngest. Feldspar from tephra layer LB7 (sample EBT-2 of Harpel et al., 2004) at the top of the Lower Barne stratigraphic section has an apparent $^{40}Ar/^{39}Ar$ age of 71 ± 5 ka (errors on ages are 2σ). Using this age and assuming a source for the ice high up on the flank of Erebus gives a minimum flow rate of 0.13–0.23 m a^{-1} for the Barne Glacier (Harpel et al., 2004). GPS surveys of three points on the lower Barne Glacier gave average flow rates of 10.92, 6.10, and 0.53 m a^{-1} (B. Bartel, unpublished data). These measured flow rates strongly suggest the Lower Barne tephra is younger than 71 ka and the sample may be contaminated with older feldspar. The Upper Barne site ranges from several hundreds of years old at the top to ≤33 ± 6 ka at the base of the section (Harpel et al., 2004). Feldspar from tephra layer UB21 (sample EBT-63 of Harpel et al., 2004) near the middle of the Upper Barne section has an apparent $^{40}Ar/^{39}Ar$ age of 15 ± 4 ka.

* Corresponding author. Department of Geosciences, 104 Wilkinson Hall, Oregon State University, Corvallis, OR, 97331-5506, USA. Tel.: +1 541 737 1201; fax: +1 541 737 1200.
E-mail address: harpelc@geo.oregonstate.edu (C.J. Harpel).

0377-0273/$ – see front matter © 2008 Elsevier B.V. All rights reserved.
doi:10.1016/j.jvolgeores.2008.06.001

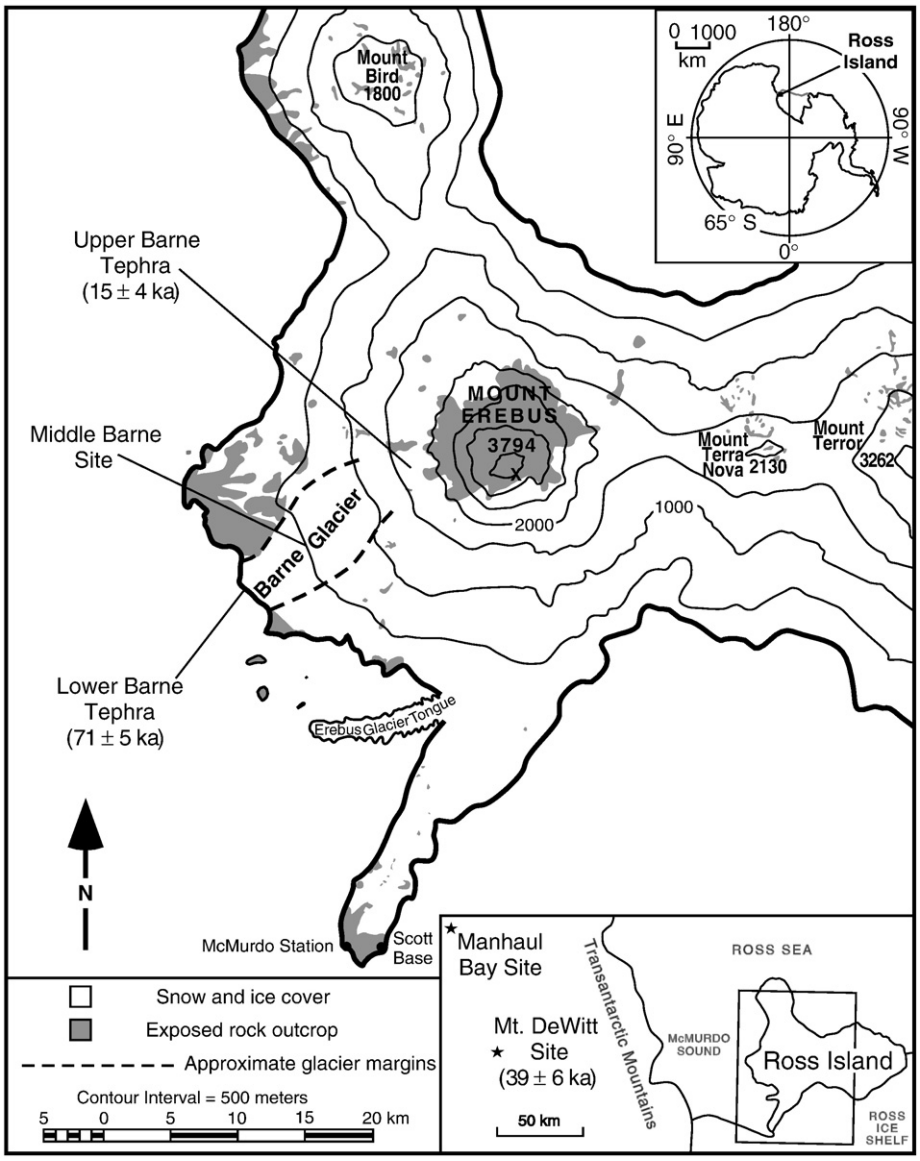

Fig. 1. Location map showing where tephra were collected.

Individual, stratigraphically unconstrained tephra were collected from ice near the summit of neighboring Mt. Terra Nova and from firn in the saddle between Mt. Terra Nova and Mt. Erebus (Fig. 1). Ash erupted from Erebus on 15 December 1997 provides a modern analog for the older englacial tephra. Distal tephra layers were found at Manhaul Bay in the Allen Hills and Mt. DeWitt, around 210 km northwest and 180 km west of Erebus volcano, respectively (Fig. 1). Dunbar et al. (1995) and Harpel (2000) preliminarily identified Erebus volcano as the source for these distal tephra layers. Feldspar from the Mt. DeWitt tephra gave an apparent $^{40}Ar/^{39}Ar$ age of 39±6 ka (Harpel et al., 2004).

2. Erebus volcano

Erebus volcano has been active since at least 1.3 Ma and has erupted lava varying from basanite to phonolite in composition (Kyle et al., 1992; Esser et al., 2004). Late Pleistocene and Holocene activity has included anorthoclase-phyric phonolitic lava flows, caldera formation, and explosive activity including a Plinian eruption forming the tephra preserved at Mt. DeWitt (Harpel et al., 2004). The lavas fill a summit caldera and form a broad annular plateau region that slopes up to the summit crater (Moore and Kyle, 1987). Volcanic activity has been confined to the summit for the last 25 ky. $^{40}Ar/^{39}Ar$ ages show that caldera-collapse events occurred between 11 ka and 25 ka and between 24 ka and 80 ka (Harpel et al., 2004; Kelly et al., 2008a-this volume). Moore and Kyle (1987) propose that these calderas were formed by piecemeal collapse without an associated large explosive eruption. However, the two distal tephra deposits indicate that Erebus volcano has definitely had large-scale explosive eruptions. An explosive origin for the young caldera must be considered because of these distal deposits.

The historic record for Erebus volcano is limited. The volcano was erupting vigorously when discovered in 1841 and both explosive activity and a possible lava flow were reported (Ross, 1847, p. 216, 220–221; Huxley, 1918, p. 112). Harpel et al. (2004), however, conclude that lava flows were unlikely at this time. Ross (1847) reported that the volcano was "emitting smoke and flame in great profusion" and "Mount Erebus was observed to emit smoke and flame in unusual quantities". Sir Joseph Dalton Hooker, the expedition scientist, further states in a letter (Huxley, 1918) that he saw a "…dark cloud of smoke tinged with flame rising from the Volcano in one column, one side jet black and the other reflecting the colors of the sun, turning off at a right

angle by some current of wind and extending many miles to leeward" most likely describing an explosive eruption and the resulting plume emitted from the volcano. Observations after discovery were sparse with detailed records beginning only around 1972. The volcano currently experiences small Strombolian eruptions from the persistent convecting anorthoclase-phonolite lava lake located in a pit crater within the summit crater (Giggenbach et al., 1973; Kyle et al., 1982; Dibble et al., 1984; Gerst et al., 2008-this volume). The eruptions periodically eject bombs onto the crater slopes over 250 m above the lava lake. Enhanced explosive activity has only been observed twice in the last 35 years. In 1984 a three month period of sustained Strombolian eruptions launched 10-m-diameter bombs more than 1 km from the vent and in 1993 two phreatic explosions excavated a small crater on the main summit crater floor (Caldwell and Kyle, 1994; Dibble et al., 1994).

The geochemical evolution of Erebus volcano is described by Kyle et al. (1992) and is constrained using $^{40}Ar/^{39}Ar$ ages (Esser et al., 2004). Detailed geochemical studies of bombs erupted between 1972 and 2004 and some older lava flows around the summit area all yield phonolite compositions and indicate that there has been no significant geochemical change within the last 25 ky (Kyle, 1977; Caldwell and Kyle, 1994; Kelly et al., 2008b-this volume; Sims et al., 2008-this volume).

The tephrostratigraphy and pre-historic explosive activity of Erebus volcano have rarely been mentioned. Lyon and Giggenbach (1974) report ash in the walls of an ice cave near the summit of the volcano and Keys et al. (1977) describe ash in firn on Fang Glacier that was believed to be up to several hundred years old. Collapse of the ice caves and subsequent snowfall have buried both of these sites. There is little evidence for pre-historic explosive activity in the geologic record because of snow and ice cover and lack of dissection on the flanks of Mt. Erebus that would typically expose stratigraphic sections. Agglomerate and tuff layers within the walls of the summit crater (Moore and Kyle, 1987) have never been studied. Panter and Winter (2008-this volume) describe a ~10-m-thick, coarse-grained, tephra-fall deposit exposed in the Side Crater and suggest formation by mixed Strombolian–phreatomagmatic eruptions.

3. Tephra field characteristics

The tephra layers are exposed as dark bands and patches in ice and firn. Where the tephra layers appear as bands they are typically tens to hundreds of meters in length. The tephra layers described here mostly occur in three groups of parallel bands in the Barne Glacier. Individual layers in these groups are separated by tens of centimeters to tens of meters of clean ice. The bands range in thickness and concentration from nearly clean ice to ~30-cm-thick layers of concentrated tephra (Fig. 2). No systematic variation of the field characteristics is noted for the tephra layers. The tephra layers are all composed of micrometer-scale shards and cannot be distinguished in the field based on shard

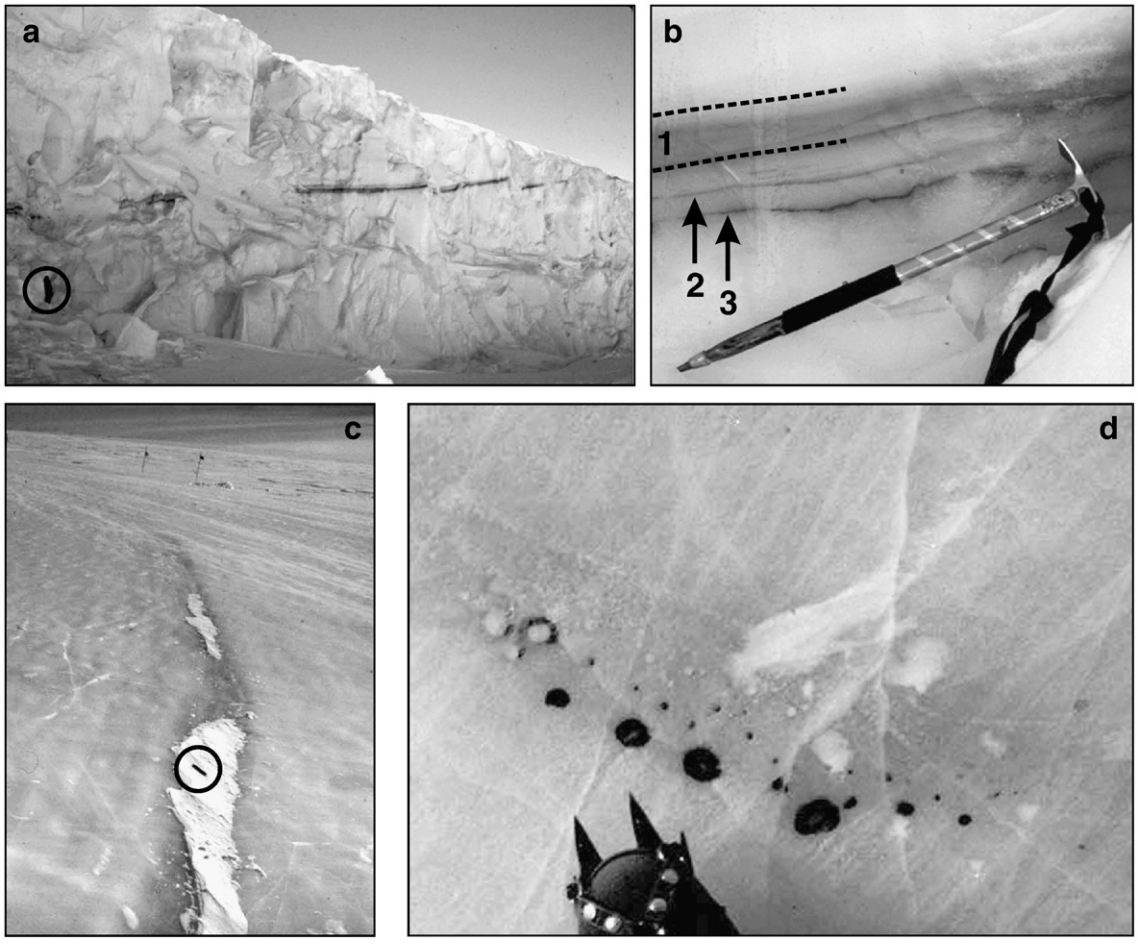

Fig. 2. Photos of in situ tephra layers within the Barne Glacier. (a) Exposure of tephra LB7 at the nose of the Barne Glacier. This tephra is one of the most concentrated tephra layers encountered. Note the person (circled) for scale. (b) Close-up photo of tephra LB7 showing that it is a composite tephra layer composed of a fine-grained, diffuse upper layer (1), thin, diffuse medial layer (2), and a coarser, concentrated basal layer (3). Variations in diffusivity of the layers could result from differing conditions during deposition and or incorporation into the ice, differences in grain size, or some combination of these factors. (c) Photo of tephra UB21 cropping out. The surface exposure of the tephra layer is slightly depressed causing snow to accumulate. This effect is caused by the dark color of the tephra layer causing differential ablation. Note the circled pen for scale on the snow. (d) A close-up photo of the surface exposure of tephra UB21. This is one of the more concentrated layers encountered and contains melt pods of tephra. The point of the crampons is ~4 cm.

Table 1
Major element compositions of glass shards in tephra from Erebus volcano

Tephra	Sample	# points	SiO_2	σ Si	TiO_2	σ Ti	Al_2O_3	σ Al	FeO	σ Fe	MnO	σ Mn	MgO	σ Mg	CaO	σ Ca	Na_2O	K_2O	σ K	P_2O_5	σ P	F	σ F	SO_2	σ S	Cl	σ Cl	Total
Mod	EBT-19	(*n*=10)	55.16	0.32	1.02	0.03	19.72	0.15	5.48	0.09	0.25	0.04	0.86	0.03	1.80	0.04	8.77	5.47	0.06	0.27	0.05	2139	963	0.08	0.02	1632	170	100.01
LB1	EBT-8	(*n*=10)	54.52	0.12	1.07	0.04	19.49	0.11	5.59	0.14	0.22	0.06	0.88	0.02	1.85	0.05	9.08	5.55	0.05	0.31	0.04	2455	978	0.09	0.01	1505	107	99.64
LB2	EBT-7	(*n*=8)	55.26	0.26	1.04	0.06	20.34	0.19	5.41	0.16	0.24	0.05	0.97	0.05	1.86	0.04	8.82	5.53	0.08	0.25	0.03	2438	993	0.07	0.02	1442	76	101.08
LB3	EBT-6	(*n*=4)	55.90	1.29	0.95	0.19	19.37	0.83	5.64	0.20	0.21	0.03	0.92	0.29	1.89	0.10	8.93	5.56	0.13	0.28	0.08	2249	669	0.08	0.04	1425	104	103.16
LB4	EBT-5	(*n*=8)	55.09	0.62	1.03	0.09	19.94	0.30	5.74	0.24	0.24	0.04	0.90	0.09	2.05	0.20	8.88	5.57	0.17	0.28	0.06	2432	673	0.09	0.03	1444	201	101.96
LB5	EBT-4	(*n*=9)	55.38	0.19	1.01	0.03	20.22	0.13	5.37	0.08	0.24	0.06	1.00	0.24	1.87	0.05	8.78	5.52	0.08	0.29	0.03	2592	941	0.09	0.03	1574	154	101.05
LB6	EBT-3	(*n*=7)	54.54	0.16	1.08	0.04	19.48	0.09	5.63	0.09	0.25	0.05	0.90	0.02	1.87	0.04	8.86	5.64	0.08	0.30	0.05	2325	628	0.08	0.02	1705	155	99.61
LB7	EBT-1	(*n*=9)	54.45	0.19	1.02	0.05	19.44	0.12	5.62	0.08	0.26	0.04	0.86	0.03	1.84	0.07	9.20	5.65	0.09	0.28	0.04	2158	452	0.07	0.02	1513	187	99.73
MB1	EBT-16	(*n*=7)	54.41	0.27	1.10	0.04	19.51	0.14	5.65	0.12	0.23	0.05	0.91	0.06	2.01	0.06	9.07	5.41	0.28	0.27	0.04	2440	733	0.08	0.01	1515	115	100.06
MB2	EBT-12	(*n*=10)	54.32	0.28	1.04	0.06	20.05	0.27	5.40	0.08	0.25	0.02	0.88	0.03	2.04	0.05	9.47	5.62	0.06	0.29	0.05	1798	931	0.08	0.02	1503	133	100.62
MB3	EBT-17	(*n*=8)	55.10	0.29	1.06	0.05	19.80	0.23	5.39	0.10	0.25	0.03	0.90	0.01	1.88	0.07	8.58	5.44	0.09	0.28	0.08	3528	2245	0.06	0.01	1569	129	100.13
MB4	EBT-9	(*n*=10)	54.43	0.17	1.01	0.02	19.56	0.13	5.55	0.13	0.24	0.06	0.87	0.03	1.84	0.05	9.34	5.50	0.06	0.27	0.06	2104	816	0.08	0.01	1563	181	99.69
MB4	EBT-10	(*n*=10)	54.37	0.15	1.03	0.05	19.56	0.08	5.60	0.09	0.25	0.05	0.87	0.03	1.85	0.03	9.28	5.53	0.08	0.28	0.03	2025	584	0.08	0.02	1536	153	99.60
MB4	EBT-18	(*n*=10)	54.60	0.16	1.03	0.05	19.51	0.08	5.53	0.12	0.28	0.05	0.87	0.02	1.85	0.06	9.06	5.58	0.10	0.30	0.05	2017	850	0.07	0.01	1623	146	99.69
UB1	EBT-41	(*n*=10)	54.42	0.22	0.99	0.02	19.90	0.13	5.47	0.20	0.26	0.06	0.87	0.06	1.90	0.05	9.39	5.62	0.08	0.29	0.04	2435	534	0.08	0.01	1578	197	100.41
UB2	EBT-40	(*n*=9)	54.36	0.21	0.98	0.05	20.09	0.08	5.50	0.09	0.24	0.07	0.84	0.04	1.93	0.07	9.22	5.68	0.13	0.30	0.03	2573	494	0.08	0.01	1599	125	100.37
UB3	EBT-40a	(*n*=10)	54.39	0.14	0.98	0.05	20.01	0.08	5.46	0.09	0.22	0.04	0.85	0.03	1.91	0.07	9.33	5.68	0.13	0.29	0.05	2717	745	0.08	0.02	1652	93	100.27
UB4	EBT-40b	(*n*=10)	54.30	0.22	1.01	0.05	20.07	0.12	5.49	0.11	0.25	0.06	0.87	0.03	1.96	0.06	9.29	5.68	0.10	0.29	0.05	2096	761	0.08	0.02	1625	138	100.41
UB5	EBT-40c	(*n*=8)	54.11	0.38	1.05	0.07	20.17	0.08	5.46	0.25	0.20	0.04	0.88	0.05	1.96	0.13	9.33	5.70	0.11	0.31	0.05	2358	832	0.09	0.02	1591	137	100.75
UB6	EBT-40d	(*n*=10)	54.40	0.28	1.03	0.04	20.08	0.19	5.45	0.10	0.25	0.04	0.96	0.11	1.98	0.06	9.09	5.62	0.05	0.30	0.03	1965	641	0.08	0.02	1537	74	100.47
UB7	EBT-39	(*n*=10)	55.11	0.29	1.02	0.06	19.67	0.16	5.62	0.11	0.25	0.03	0.87	0.03	1.85	0.08	9.11	5.58	0.09	0.31	0.03	2424	914	0.07	0.02	1537	171	100.72
UB8	EBT-36	(*n*=7)	54.84	0.37	1.04	0.04	19.97	0.10	5.36	0.09	0.21	0.05	0.89	0.01	1.92	0.07	8.78	5.42	0.12	0.27	0.05	2695	548	0.09	0.01	1885	173	100.08
UB9	EBT-35a	(*n*=7)	55.28	0.16	1.08	0.06	19.96	0.11	5.48	0.08	0.27	0.04	0.96	0.02	2.00	0.06	8.10	5.36	0.07	0.29	0.03	1961	712	0.08	0.02	1814	277	99.84
UB10	EBT-35b	(*n*=8)	54.80	0.36	1.08	0.05	19.94	0.32	5.51	0.06	0.26	0.06	0.96	0.05	2.04	0.13	8.48	5.44	0.04	0.31	0.03	1962	558	0.08	0.02	1660	119	100.33
UB11	EBT-35	(*n*=8)	55.29	0.40	1.09	0.06	20.10	0.27	5.41	0.15	0.24	0.05	0.93	0.04	1.97	0.08	7.97	5.47	0.04	0.29	0.05	1833	785	0.08	0.02	2062	359	100.33
UB11	EBT-38	(*n*=10)	54.06	0.22	1.07	0.03	20.12	0.14	5.54	0.09	0.25	0.05	0.90	0.04	2.08	0.04	9.31	5.59	0.09	0.29	0.04	2118	1020	0.09	0.04	1587	288	100.36
UB12	EBT-34d	(*n*=9)	54.57	0.28	1.06	0.07	19.63	0.13	5.66	0.12	0.28	0.06	0.90	0.16	2.00	0.07	9.17	5.61	0.11	0.30	0.04	2026	811	0.08	0.02	1429	130	100.60
UB13	EBT-34c	(*n*=10)	55.06	0.33	1.05	0.07	20.33	0.51	5.42	0.40	0.22	0.07	0.98	0.02	1.98	0.06	8.89	5.55	0.10	0.27	0.02	2129	480	0.08	0.02	1440	89	101.76
UB14	EBT-34b	(*n*=10)	55.19	0.31	1.05	0.05	20.21	0.05	5.48	0.13	0.25	0.08	0.95	0.08	1.98	0.06	8.97	5.43	0.12	0.28	0.03	1872	512	0.08	0.03	1381	169	101.07
UB15	EBT-34a	(*n*=6)	55.01	0.30	1.07	0.06	19.86	0.12	5.31	0.12	0.20	0.06	0.91	0.02	1.99	0.05	8.83	5.36	0.13	0.29	0.04	1901	534	0.08	0.01	1873	1021	100.14

UB16	EBT-34	(n=5)	55.00	0.17	1.09	0.07	20.07	0.18	5.50	0.07	0.21	0.07	0.96	0.01	1.97	0.07	8.23	5.36	0.06	0.31	0.05	2984	978	0.08	0.00	1689	160	99.93
UB16	EBT-37	(n=7)	54.65	0.51	1.10	0.06	19.89	0.29	5.45	0.18	0.25	0.06	0.93	0.02	1.99	0.08	8.74	5.41	0.07	0.29	0.03	2786	775	0.08	0.01	2146	652	100.53
UB17	EBT-33	(n=5)	55.02	0.54	1.12	0.08	19.88	0.17	5.47	0.05	0.26	0.08	0.80	0.35	2.00	0.04	8.46	5.39	0.10	0.33	0.02	2421	689	0.09	0.01	1887	203	100.66
UB18	EBT-32a	(n=10)	55.02	0.18	1.09	0.05	19.75	0.18	5.65	0.11	0.24	0.02	0.90	0.02	2.00	0.04	9.02	5.48	0.08	0.30	0.03	1962	881	0.08	0.01	1597	206	100.57
UB19	EBT-32	(n=10)	54.98	0.26	1.09	0.04	19.73	0.14	5.66	0.19	0.23	0.05	0.91	0.03	2.00	0.08	9.09	5.46	0.07	0.28	0.03	2259	779	0.08	0.01	1535	102	100.74
UB20	EBT-54	(n=10)	54.32	0.23	1.03	0.04	20.17	0.10	5.49	0.13	0.22	0.07	1.01	0.28	2.02	0.07	9.22	5.62	0.09	0.31	0.05	2195	569	0.08	0.02	1469	82	100.86
UB21	EBT-30	(n=10)	54.46	0.35	1.03	0.05	20.12	0.16	5.50	0.07	0.22	0.03	0.80	0.26	2.06	0.04	9.23	5.61	0.09	0.28	0.04	2135	654	0.08	0.02	1442	127	100.79
UB21	EBT-53	(n=10)	54.23	0.21	1.04	0.05	20.22	0.20	5.45	0.05	0.24	0.08	0.89	0.03	2.04	0.06	9.24	5.71	0.06	0.31	0.04	2380	740	0.09	0.01	1560	87	100.59
UB22	EBT-52	(n=10)	54.32	0.31	1.07	0.04	20.16	0.14	5.49	0.11	0.23	0.06	0.92	0.02	2.05	0.07	9.09	5.73	0.09	0.31	0.03	2227	632	0.09	0.02	1574	128	100.68
UB23	EBT-51	(n=10)	54.41	0.15	1.06	0.02	19.98	0.08	5.47	0.04	0.21	0.03	0.93	0.03	2.02	0.05	9.07	5.66	0.08	0.32	0.05	2113	449	0.09	0.02	1545	117	100.08
UB24	EBT-50	(n=10)	54.28	0.20	1.06	0.04	19.89	0.15	5.50	0.08	0.25	0.05	0.90	0.03	2.07	0.12	9.19	5.67	0.11	0.31	0.03	2428	1516	0.08	0.01	1546	76	100.39
UB25	EBT-49	(n=10)	54.27	0.34	1.07	0.04	19.80	0.35	5.49	0.09	0.22	0.06	0.94	0.03	2.08	0.07	9.31	5.66	0.09	0.33	0.04	2100	741	0.08	0.02	1586	90	100.69
UB26	EBT-48	(n=10)	54.14	0.12	1.06	0.03	20.04	0.13	5.47	0.09	0.28	0.06	0.96	0.08	2.02	0.05	9.26	5.66	0.09	0.31	0.02	1887	933	0.08	0.02	1465	158	100.25
UB27	EBT-47	(n=9)	54.61	0.16	1.06	0.03	19.93	0.07	5.45	0.04	0.24	0.04	0.91	0.04	2.00	0.08	9.13	5.62	0.09	0.28	0.04	1447	1037	0.07	0.01	1568	85	100.17
UB28	EBT-23a	(n=9)	54.30	0.21	1.07	0.05	19.76	0.10	5.53	0.09	0.21	0.05	0.92	0.03	2.07	0.05	9.59	5.52	0.09	0.30	0.02	2710	854	0.09	0.01	1350	103	100.44
UB28	EBT-23b	(n=10)	54.02	0.36	1.09	0.04	19.96	0.25	5.57	0.09	0.24	0.05	0.90	0.04	2.11	0.05	9.56	5.53	0.11	0.32	0.04	2162	695	0.09	0.02	1532	140	100.76
UB29	EBT-22	(n=7)	54.35	0.37	1.05	0.03	19.93	0.13	5.50	0.12	0.26	0.05	0.90	0.03	2.01	0.10	9.36	5.61	0.09	0.30	0.04	2332	522	0.09	0.01	1615	160	100.68
UB30	EBT-21	(n=6)	54.09	0.26	1.04	0.05	19.85	0.13	5.51	0.08	0.28	0.03	0.89	0.01	2.06	0.09	9.65	5.60	0.16	0.32	0.06	2365	862	0.09	0.01	1516	210	100.58
SD	EBT-43	(n=9)	55.45	0.16	1.01	0.05	20.30	0.13	5.35	0.13	0.23	0.06	0.90	0.05	1.83	0.03	8.99	5.47	0.07	0.24	0.05	1967	439	0.08	0.02	1493	112	100.88
SD	EBT-44	(n=9)	55.15	0.34	1.00	0.04	20.25	0.20	5.46	0.09	0.25	0.03	0.99	0.17	1.71	0.48	9.19	5.50	0.26	0.28	0.04	1924	685	0.09	0.04	1379	114	101.82
SD	EBT-45	(n=10)	55.48	0.29	1.02	0.06	20.22	0.15	5.34	0.21	0.26	0.05	0.87	0.05	1.87	0.04	8.90	5.54	0.15	0.23	0.05	2254	1182	0.09	0.04	1449	141	101.18
TB7	EBT-56	(n=4)	54.55	0.21	1.01	0.04	19.56	0.08	5.60	0.09	0.25	0.08	0.88	0.02	1.90	0.05	9.00	5.56	0.07	0.30	0.03	2088	80	0.06	0.01	1603	108	99.69
TN	EBT-62	(n=7)	55.04	0.29	0.98	0.05	19.88	0.24	5.54	0.17	0.29	0.07	0.85	0.05	1.88	0.05	9.24	5.31	0.44	0.28	0.06	2132	1077	0.07	0.02	2244	905	101.16
MH	BIT-42	(n=10)	54.91	0.23	1.00	0.04	19.88	0.14	5.57	0.11	0.24	0.05	0.84	0.04	1.97	0.10	9.03	5.61	0.21	0.26	0.04	2326	751	0.08	0.03	1568	131	100.70
DW	BIT-272	(n=10)	55.53	0.27	0.95	0.04	19.51	0.07	5.91	0.09	0.28	0.05	0.80	0.01	1.91	0.04	8.74	5.51	0.15	0.24	0.04	1807	807	0.08	0.02	1345	137	100.49
DW	BIT-288	(n=10)	55.56	0.23	0.95	0.04	19.51	0.09	5.86	0.12	0.26	0.04	0.80	0.03	1.93	0.04	8.69	5.51	0.06	0.26	0.04	1964	854	0.09	0.03	1385	200	100.41

Notes: Analyses made by Cameca SX-100 electron microprobe at New Mexico Tech. Glass was analyzed using a defocused 25 μm beam to mitigate Na_2O loss (Hunt and Hill, 1993) and a beam current of 10 nA. An accelerating potential of 15 keV was used for all analyses. Counts on peak were 20 s for all elements except Na, Cl, and F, which were counted at 40, 40, and 100 s, respectively. No σ is reported on Na_2O as only one analysis per sample is used. The Berkeley 310 Albite and Berkeley 374 Orthoclase feldspar standards and VG568 rhyolite, KN18, and KE12 glass standards were analyzed during each analytical session to monitor the accuracy of microprobe calibration. Oxides are reported as weight percent with Cl and F reported in ppm. Typical analytical precision for microprobe analyses is represented by the standard deviation of replicate analyses of standard VG568, KN18, and KE12: SiO_2 (0.47 wt.%), TiO_2 (0.03 wt.%), Al_2O_3 (0.18 wt.%), FeO (0.06 wt.%), MnO (0.06 wt.%), MgO (0.07 wt.%), CaO (0.02 wt.%), Na_2O (0.55 wt.%), K_2O (0.27 wt.%), P_2O_5 (0.02 wt.%), F (1910 ppm), SO_2 (0.01 wt.%), Cl (67 ppm).

characteristics or componentry of the tephra. The dark-colored tephra decrease the albedo of the ice and absorb sunlight consequently increasing ablation and causing the surface exposure of the tephra to be slightly depressed relative to the clean ice surface (Fig. 2). In highly concentrated tephra layers, small pods of tephra, referred to as melt pods, may be present just below the surface of the ice (Fig. 2). These pods were formed by the redistribution of the tephra in the ice during melting and ablation caused by solar heating.

4. Methods

4.1. Samples

We collected 56 tephra samples representing 46 individual layers. Each tephra sample is identified by sample location and when applicable a number related to stratigraphic position. Identifications are; UB for Upper Barne, MB for Middle Barne, LB for Lower Barne, SD for Erebus saddle, TN for Terra Nova, MH for Manhaul Bay, and DW for DeWitt (Fig. 1). Stratigraphic position is represented with 1 being the highest tephra in the section and hence youngest and numbers increase with age. Thus, tephra LB1 is the youngest tephra at the Lower Barne site.

All tephra samples were obtained from blue ice except for UB1 and SD, which occur in firn. The tephra from the December 2007 eruption was collected from a clean snow surface. In the field small samples of ice (~1–3 kg) were initially chipped from surface exposures to get reconnaissance tephra samples. Later larger ice samples, ranging from ~25 to ~365 kg, were taken using a chainsaw to cut blocks of tephra-bearing ice from the glacier. These larger samples were taken from layers that contained highly concentrated tephra in the hope that anorthoclase could be separated and the tephra dated (see Harpel et al., 2004). The ice was melted, the water decanted, and the tephra air-dried.

4.2. Scanning electron microscopy

Scanning electron microscopy images were collected using the electron microprobe described in the notes for Table 1. Tephra samples were sprinkled onto double-sided carbon tape adhering to a glass slide then evaporatively coated with carbon. Imaging was done using an accelerating potential of 15 keV and a beam current ranging from 0.05 to 1 nA.

4.3. Geochemistry

Chemical compositions of fresh glass in the tephra were determined by electron microprobe on polished grain mounts. Analytical details are given in Table 1. Usually 10 shards were analyzed in each sample (data for individual shards available in Harpel, 2000). Major element analyses typically totaled between 98 and 102 wt.%. Analyses outside this range were excluded except for sample EBT-62 where the fine grain size necessitated the use of analyses with totals as low as 93 wt.%. The final composition for each tephra was calculated by averaging the analyses from each shard except for Na_2O. In each sample the highest measured Na_2O content was used as a way to lessen the effect of Na loss due to heating by the electron beam. All analyses were normalized to 100 wt.%.

Between 2 and 5 feldspar crystals were analyzed from each tephra sample. Feldspar compositions were considered individually to detect the presence of contamination within the sample. Trace element concentrations of selected whole tephra samples were determined by instrumental neutron activation analysis (INAA); details are given in Table 2.

5. Results

5.1. Scanning electron microscopy

The relative abundance of key shard morphologies (*i.e.* blocky, pumice, etc.) and grain size distributions were recorded for each tephra sample (Table 3). Sheridan and Marshall (1983) showed that qualitative analyses could be an effective way to determine the eruption mechanism for tephra. We have therefore used qualitative characterization of shard morphologies to determine eruption mechanisms. As the samples are fine-grained and well sorted the full grain size distribution of each tephra could be observed using SEM and backscattered electron images. Relative sorting, vesicularity, and the relative abundances of glass, crystals, and lithics were estimated for each tephra. Anorthoclase feldspar is the dominant crystal phase with minor apatite, olivine, Fe–Ti oxide, and sulfide phases. Lithic fragments were present in varying quantities and were recognized by their rough surface morphology.

Shard morphologies are subdivided into two groups. In group one, 24 tephra samples are composed of blocky and platy shards with low vesicularity (Fig. 3). Vesicles, when present, are truncated. Mossy and hackled shards are also relatively common with chemical pitting, hydration rinds, sublimate coatings, and dust-and-sublimate filled cavities occurring less frequently (for comparable textures see: Wohletz, 1983; Heiken and Wohletz, 1985; Büttner et al., 1999; Dellino et al., 2001). Microscopic accretionary lapilli-like aggregates are also rarely present. In group two, 5 tephra samples are characterized by their high degree of vesiculation and the presence of fluidal and torn shards and Pele's hair (Duffield et al., 1977; Heiken, 1978; Heiken and Wohletz, 1985, p.25–28) (Fig. 4). Woody pumice-like shards are included in this group. Nineteen of the tephra contain shard morphologies characteristic of both groups.

Several notable features are found in the tephra. Droplets ranging from spherical to subrounded and shards with “budding” morphology are found in some of the samples (Fig. 5). Budding morphology is defined as a main melt globule covered with bulbous droplets in varying stages of disaggregation or coalescence.

Clasts with zeolite and clay encrustations are found in many tephra samples. In 15 of the samples small clusters of and rare individual crystals were found that have excellent crystal form (Fig. 6). Typically these clumped crystals are cubic with trapezohedral terminations but rarely they are trapezohedral. The crystals are usually ~20 μm in diameter and rarely ≥50 μm. Qualitative elemental scans by electron microprobe show the crystals are primarily composed of Na, Al, and Si. The crystals are identified as analcime by their chemistry and crystal habit.

The analcime crystals are often intimately associated with other zeolites (Fig. 6), which are typically ≤10 μm and exhibit diverse crystal habits. The zeolites have not been identified to specific type. Some undifferentiated clay minerals are also present and are occasionally intermixed with the zeolites. Rarely an amorphous phase is observed, similar to that described by de'Gennaro et al. (2000).

The distal tephra layers from Manhaul Bay and Mt. DeWitt, are both poorly sorted on the SEM images. They contain abundant feldspar and clearly differ from the more proximal tephra samples. The Manhaul Bay tephra is weakly vesiculated and composed primarily of platy and blocky shards with occasional bubble wall shards. The glass shards commonly have chipped edges. The Mt. DeWitt tephra mostly has bubble wall shards with subordinate platy shards and rare pumice.

5.2. Geochemistry

All of the tephra have phonolitic glass compositions with an average of ~55 wt.% SiO_2 and 13.5 wt.%–15.3 wt.% total alkalis (Na_2O+K_2O) (Table 1; Fig. 7). Some Na_2O loss may have occurred during microprobe analysis (Hunt and Hill, 1993) as discussed below but it is not considered to be a significant problem. The Na_2O concentrations in glass shards are consistently higher than those measured using INAA on bulk tephra samples (Table 2). As the bulk samples are diluted by crystals they should have a lower Na_2O concentration than the glass. If significant Na_2O loss had occurred during microprobe analyses concentrations would be lower than those obtained using INAA.

The major element compositions of glass shards show only minor variations (Fig. 7). SiO_2 varies between 54 and 56 wt.% and there is an apparent negative correlation between SiO_2 and Na_2O+K_2O (Fig. 7),

Table 2
Geochemical data from INAA of bulk tephra samples

Tephra	Sample	Na_2O	Sc	FeO	Co	Zn	As	Br	Rb	Sr	Sb	Cs	Ba	La	Ce	Nd	Sm	Eu	Tb	Yb	Lu	Hf	Ta	Th	U
Mod	EBT-19	7.85	2.69	5.13	2.25	157	10.3	4.9	132	258	0.47	1.86	473	149.0	287.4	97.5	17.31	3.59	2.07	6.45	0.981	27.92	24.50	26.33	6.90
LB1	EBT-8	8.42	2.75	5.26	2.88	137	2.6	3.3	112	785	0.34	1.45	836	136.4	261.6	87.3	15.67	4.44	1.88	6.00	0.803	23.28	17.67	22.05	7.59
LB7	EBT-1	8.61	2.79	5.23	2.43	154	5.0	3.9	136	427	0.32	1.80	621	148.0	284.7	107.6	17.54	3.88	2.08	6.78	0.997	27.15	20.03	25.88	6.61
LB7	EBT-56	8.33	3.00	5.40	3.16	162	4.8	3.8	130	456	0.53	1.80	581	145.7	276.8	95.0	17.22	3.75	2.07	6.46	0.914	26.50	19.15	24.91	6.92
MB3	EBT-17	8.31	3.17	6.13	3.67	170	3.3	3.4	128	476	0.70	1.59	628	149.0	287.0	98.9	17.55	4.03	2.12	6.62	0.963	26.16	19.20	24.23	8.25
MB4	EBT-18	8.07	2.91	5.65	2.57	166	9.4	4.7	123	471	0.67	1.84	688	148.7	287.4	100.9	17.64	4.13	2.13	6.69	0.912	26.11	20.14	25.10	6.74
UB1	EBT-41	8.99	2.86	5.42	2.13	158	3.1	4.2	145	234	0.44	1.87	535	160.7	309.0	113.3	18.97	3.75	2.23	7.50	1.032	29.77	22.10	28.37	8.83
UB2	EBT-40	8.17	2.85	5.55	2.55	155	6.7	4.3	129	454	0.41	1.86	660	152.1	289.4	104.0	17.74	4.11	2.14	6.50	0.922	26.64	20.00	25.02	7.14
UB4	EBT-40b	8.66	2.92	5.84	2.93	172	4.5	4.1	133	402	0.34	1.68	626	153.7	297.9	105.4	17.75	4.08	2.17	6.93	0.963	26.99	20.03	25.60	8.50
UB6	EBT-40d	8.67	2.84	5.39	2.34	159	7.8	4.3	144	337	0.48	1.88	493	156.0	300.0	107.0	18.17	3.74	2.23	6.92	1.052	29.10	22.06	27.82	8.06
UB8	EBT-36	8.73	2.73	5.21	2.39	152	4.1	4.8	140	381	0.40	1.80	639	150.2	288.3	102.0	17.29	3.80	2.08	6.85	0.965	27.70	20.50	25.92	8.02
UB9	EBT-35A	8.65	2.88	5.58	2.57	150	5.7	4.8	136	302	0.52	1.86	574	155.7	306.0	101.9	18.39	3.84	2.20	7.10	0.966	28.78	21.72	27.53	8.07
UB11	EBT-38	8.53	2.87	5.63	3.16	172	6.4	3.8	134	343	0.56	1.81	510	153.3	293.9	101.3	17.89	3.73	2.09	7.02	1.023	28.50	21.10	26.60	9.20
UB16	EBT-37	8.73	2.86	5.60	2.93	166	3.5	4.3	138	333	0.43	1.84	546	152.9	299.3	97.0	17.60	3.76	2.18	6.96	0.984	28.70	21.32	27.26	7.83
UB20	EBT-54	8.56	2.90	5.64	2.68	164	7.7	3.9	138	293	1.79	1.97	533	155.8	304.0	100.0	18.13	3.79	2.23	7.01	0.962	28.50	21.67	27.34	7.63
UB21	EBT-53	8.41	2.64	5.30	2.76	153	4.5	4.0	124	542	0.55	1.64	716	146.7	280.0	101.6	16.86	4.12	2.01	6.52	0.913	25.64	18.88	24.16	7.18
UB22	EBT-52	8.51	2.93	5.44	3.26	224	5.6	3.9	130	488	6.72	–	712	147.5	283.1	95.3	17.32	4.08	2.09	6.49	0.918	26.18	19.71	24.96	7.59
UB23	EBT-51	8.58	2.86	5.50	2.70	197	6.2	4.3	140	334	0.66	1.78	567	155.3	299.2	105.2	18.24	3.75	2.16	7.08	1.023	29.00	21.30	26.94	8.06
UB24	EBT-50	8.27	3.06	5.51	3.97	315	8.1	5.1	137	356	2.12	1.80	587	150.8	293.5	101.0	17.35	3.72	2.13	6.88	0.977	28.00	21.13	26.57	8.24
UB25	EBT-49	8.52	2.85	5.51	2.87	166	5.3	4.4	136	477	3.14	1.79	603	155.2	298.8	104.7	18.11	3.93	2.19	7.22	0.974	27.81	20.45	26.31	9.00
UB26	EBT-48	8.57	2.85	5.57	2.91	174	6.8	4.8	135	314	1.90	1.88	537	153.9	298.3	100.0	18.06	3.80	2.20	6.68	1.025	28.60	21.82	27.47	7.51
UB27	EBT-47	8.21	3.20	5.65	3.29	309	9.2	4.3	125	426	3.57	1.76	659	151.3	285.8	105.2	17.98	3.90	2.10	6.70	0.969	27.41	20.30	26.10	7.83
MH	BIT-42	8.18	2.30	4.73	2.35	133	4.4	2.5	102	836	0.67	1.43	1199	139.0	271.0	99.0	16.58	5.28	1.96	5.65	0.804	21.00	15.33	19.34	5.80
DW	BIT-288	8.41	2.79	4.78	2.27	135	3.7	3.5	114	722	1.50	1.37	1038	138.4	270.3	102.0	17.12	5.01	2.00	5.97	0.815	22.50	16.00	20.35	6.70
Precision		0.01	0.06	0.03	0.15	2	0.2	0.2	2	54	0.04	0.04	13	0.2	0.9	2.0	0.13	0.02	0.03	0.05	0.009	0.20	0.01	0.10	0.10

Notes: Trace element, FeO, and Na_2O concentrations were determined for ~100 mg whole tephra samples. Samples were sealed into high purity quartz vials and irradiated at the University of Missouri research reactor for 24 h under an average neutron flux of 2.5×10^{13} n cm^{-2} s^{-1}. All analyses were counted at the New Mexico Tech using two coaxial p-type high purity Ge detectors with resolutions of 1.8 keV at 1332 keV and 0.6 keV at 122 keV (as detailed in Hallett and Kyle, 1993). A total of 8192 channels of spectra data were collected using a Nuclear Data 9900 system and reduced by the TEABAGS (Trace Element Analysis By Automated Gamma-ray Spectrometry) program (Lindstrom and Korotev, 1982) using a Digital VAXstation 3100 computer. Samples were counted between 6 to 12 days and again at 30 to 45 days after irradiation. Standard NIST SRM 1633a (coal-fly ash) was used as a reference standard for all of the elements except Na_2O, where USGS Rock Standard G-2 was used. Oxides are reported as weight percent and all other elements are reported in ppm. Analytical precision was determined using four aliquots of the intralaboratory Antarctic tephra standard BIT-110: Na_2O (0.01 wt.%), Sc (0.06 ppm), FeO (0.03 wt.%), Co (0.15 ppm), Zn (2 ppm), As (0.2 ppm), Br (0.2 ppm), Rb (2 ppm), Sr (54 ppm), Sb (0.04 ppm), Cs (0.04 ppm), Ba (13 ppm), La (0.2 ppm), Ce (0.9 ppm), Nd (2.0 ppm), Sm (0.13 ppm), Eu (0.02 ppm), Tb (0.03 ppm), Yb (0.05 ppm), Lu (0.009 ppm), Hf (0.20 ppm), Ta (0.01 ppm), Th (0.10 ppm), and U (0.10 ppm).

which may be an analytical artifact. When Na loss occurs during microprobe analyses there is a systematic increase in SiO_2, which could explain the trend. No other elements show any correlation with SiO_2 and there is general scatter in the data, which is close to the analytical uncertainties of the elements in question.

When the major element concentrations of the UB and a modern (1997) tephra are plotted in stratigraphic order some minor trends are apparent (Fig. 8). The top of the UB section is estimated to be a few hundred years old so there is only a short time break to the 1997 tephra. There is a decrease in CaO in glasses as the UB tephra become younger and this continues to the modern tephra. More subtle decreases in P_2O_5 and SO_2 also occur as the tephra become younger. FeO, MgO and MnO show no trends with time. The negative correlation between SiO_2 and alkalies shows up well in the stratigraphic plots and so the prominent spikes of increased SiO_2 and decreased Na_2O+K_2O may be analytical. Ignoring the large spikes, SiO_2 increases up-section and then decreases toward the top. The alkalies show the opposite pattern and reach their lowest levels in the middle of the section. The Al_2O_3 concentrations are scattered but overall there is a subtle increase up-section which shows the opposite trend to CaO (Fig. 8). If the composition of the modern tephra is considered it shows that the trends of CaO and Al_2O_3 may continue through to 1997.

Analyses of glass in 2 samples of the Mt. DeWitt tephra are identical but they differ from glass in the other distal tephra from Manhaul Bay (Table 1; Fig. 7). Therefore the 2 distal tephra are unlikely to be correlative and probably represent 2 separate eruptions. The Mt. DeWitt glass has higher SiO_2 and FeO and lower MgO, TiO_2, and Al_2O_3, which distinguishes it from the other glass analyses. The Manhaul Bay glass is compositionally similar to glasses from proximal locations.

Trace element concentrations of bulk samples show a slight enrichment in LREE in an OIB normalized trace element pattern (Fig. 9a) but no significant systematic variations exist among samples. The tephra are depleted in Ba and Sr and have very slight negative Eu anomalies in a chondrite normalized trace element diagram (Fig. 9b). Tephra LB1 lacks a Eu anomaly and the two distal tephra have slight positive Eu anomalies and are less depleted in Ba and Sr than the proximal tephra samples.

Trace element concentrations are affected by the amount of feldspar in the tephra. Elements that are incompatible in feldspar show positive correlations with each other (e.g. Fig. 10). Sr, Ba, and Eu, which are compatible in feldspar, show well-defined negative correlations with incompatible elements such as Th. Because the feldspar dilutes the concentration of incompatible elements the amount of feldspar in a sample can be calculated from the correlations (Fig. 10). The trace element data suggest the 2 distal tephra have over 25% more feldspar than the most feldspar-poor proximal tephra. The enrichment in feldspar is consistent with the positive Eu anomaly exhibited by both samples.

Anorthoclase is the dominant feldspar in the tephra (Fig. 11). Minor plagioclase and sanidine crystals also occur. The alkali feldspars range from anorthoclase ($An_{24}Or_{10}$) to sanidine (An_2Or_{50}). The sanidine is similar to those reported in Erebus anorthoclase phonolite (Kyle et al., 1992) and is considered to be juvenile. All of the feldspars analyzed from the distal tephra are juvenile anorthoclase ($An_{17}Or_{18}$–$An_{10}Or_{25}$) (Fig. 11). The plagioclase are outside of the reported feldspar compositions for Erebus anorthoclase phonolite but are within the range of those reported by Kyle et al. (1992) for more basic Erebus Lineage lavas. The plagioclases are likely xenocrysts but are most likely locally derived.

6. Eruption characteristics

6.1. Eruption mechanisms

The proximal phonolitic tephra layers were formed by both phreatomagmatic and Strombolian eruptions. Wohletz (1983) found

Table 3
Abundances of tephra components, grain size distribution, morphological features, and eruption type of Erebus englacial tephra

Tephra	Sample	Modal distribution					Grain size (μm)			Phreatomagmatic textures									Strombolian textures						Other				
		Glass	Crystal	Lithic	Vesicularity	Sorting	Max	Av	Min	Blocky	Platy	Mossy	Hackly	Accretionary lapilli	Hydration rind	Quench cracks	Chemical pitting	Sublimate	Torn	Pumice	Fluidal	Droplets	Welded droplets	Budding	Pele's hair	Anal-cime	Clay and zeolites	Amorphous silica	Eruption mode
Modern	EBT-19	P	S	S	High	Poor	465	150	45	C	C				X	X	X	X	O	R	O				O	X	X	X	Pm
LB1	EBT-8	P	F	S	Low	Poor	400	60	25	A	O									R	O	O	X	X			X		Pm
LB2	EBT-7	P	F	S	Mod.	Mod.	270	90	45	A	O		X									R							Pm/S
LB3	EBT-6	S	S	P	Low	Well	270	90	30	A				X	X														Pm
LB6	EBT-3	P	F		Low	Well	280	170	57	A	R									R	R								Pm
LB7	EBT-1	P	S	S	High	Mod.	500	200	30	O	O	R							A	C					R	X	X		S
LB7	EBT-2				Mod.	Poor	460	170	10	C									A	C	O					X	X		S
LB7	EBT-56	P	S	S	Mod.	Poor	230	70	20	A									C	O		R			R	X			S
MB1	EBT-16	F	F	F	Low	Poor	580	135	30	C	C	A			X	X	X	X					X		R	X?	X	?	Pm
MB2	EBT-12	P	S	S	Mod.	Mod.	660	360	165	A	O					X			R			R	X						S/Pm
MB3	EBT-17	P	S	S	Mod.	Mod.	460	170	25	A	A	O					X		R	R	O								Pm
MB4	EBT-9	F	S	F	Mod.	Mod.	300	175	30	A	O	O		X						O	O					X	X		S/Pm
MB4	EBT-10	P	S	F	High	Mod.	280	120	30	C	C			R		X	X		O	C	R	O	X			X	X		S/Pm
MB4	EBT-18	F	F	F	High	Poor	115	140	20	C	A									O	O					?	X		Pm
UB1	EBT-41	P	S	S	High	Mod.	1210	260	100	C	O				X?		X		C	C	C						X		S
UB2	EBT-40	P	S	S	Mod.	Poor	600	110	10	C	C	O		O	X			X	C	O	O	R	X		R	X	X		S/Pm
UB4	EBT-40b	P	S	S	Mod.	Mod.	610	110	35	A	C		X		X			X	R	R		R		X	R		X		Pm
UB5	EBT-40c	P	S	S	Mod.	Mod.	650	165	85	A	C		X						O				X			X	X		Pm/S
UB6	EBT-40d	P	S	S	High	Poor	1110	110	20	O	C				X	X			C	O	C		X	X	O		X		S/Pm
UB6.5	EBT-40f					Well	430	175	40	A	C			X?	X?			X			O	R	X						Pm
UB7	EBT-39	P	S	F	Low	Well	500	130	75	A	C	R						X			R		X						Pm
UB8	EBT-36	P	S	S	Low	Mod.	580	180	55	A								X	C	O	O	R			R				Pm
UB9	EBT-35a	P	S	S	Mod.	Mod.	525	180	70	C	C		X					X	C	O	C								S/Pm
UB10	EBT-35b	P	S	S	Mod.	Mod.	775	240	40	C									C	R	O								S/Pm
UB11	EBT-35	P	F		Mod.	Mod.	590	200	90	C	C								R	C	O		X		R				S/Pm
UB11	EBT-38	P	S	S	Low	Poor	435	120	40	A	A		X		X			X	O	O	R		X		R				Pm
UB13	EBT-34c	P	S	S	Mod.	Poor	680	130	90	A						X			C	O	O						X		Pm

UB14	EBT-34b	F	F	S	Low	Well	290	140	85	A	C	R				X		X							X				X			Pm
UB15	EBT-34a	P	F		Low	Low	675	135	55	A											A	C	R									Pm
UB16	EBT-34	P	S		Mod.	Mod.	790	235	120	O	A										O	C	C									S/Pm
UB16	EBT-37	P	S	S	Mod.	Poor	550	90	30	C	A		X								O	O	O									S/Pm
UB16.5	EBT-33a				Low	Well	430	160	50	A	O	O	X			X						R	R						X	?		
UB17	EBT-33	P	S	S	Mod.	Mod.	490	150	60	A	C								X		O	R	C						X	X	S
UB18	EBT-32a				Low	Mod.	430	200	85	C	C					X		X			O	O	C						X			Pm
UB19	EBT-32	P	S	S	Mod.	Mod.	750	230	115	A	C	O						X				R	O						X			S/Pm
UB20	EBT-54	P	S	S	High	Poor	650	150	20	C	C					X					C	C		C	X		O	?	X			S
UB21	EBT-53	P	S	F	Poor	Poor	690	135	10	A	C			R		X					O	O		C	X		R	X	X			Pm
UB21	EBT-30	P	S	S	Mod.	Mod.	430	120	47	C	C	R							X		O	O	O	R			R		X			S/Pm
UB22	EBT-52	P	S	S	Low	Well	335	140	20	A	O							X						O	X		R		X			Pm/S
UB23	EBT-51	P	S	S	High	Mod.	360	125	30	C	C							X			O	O		O	X	X	O					S/Pm
UB24	EBT-50	P	S	S	Mod.	Well	385	170	40	C	C					X					R	O	R	R			R	X	X			S/Pm
UB25	EBT-49	P	S	S	Mod.	Poor	435	160	20	C	A					X				X	R	R			X	X	R	X	X			S/Pm
UB26	EBT-48	P	S	S	High	Mod.	620	140	30	C	C					X		X	X		O	O	O		X	X	R			X		S/Pm
UB27	EBT-47	P	S	S	Mod.	Mod.	630	90	30	C	C							X		X	R		R	R	X			X	X			S/Pm
UB28	EBT-23a	P	S	S	Mod.	Mod.	525	140	30	A	C	O								X	R		O		X							Pm
UB28	EBT-23b	P	S	S	low	mod.	460	115	55	A	C	R											O										Pm
UB29	EBT-22	P	S		mod.	mod.	370	115	30	C	C	A															R		X				Pm
UB30	EBT-21	F	F	F	low	poor	510	150	15	A	C																						Pm
UB30	EBT-40a	P	S		low	mod.	460	110	40	C	C			X		X			X		O		R	O	X							Pm
SD	EBT-43	P	S	S	mod.	mod.	285	90	20	C	O							X			A			O	X				X			Pm/S
SD	EBT-44	P	S	S	mod.	mod.	440	90	15	A	A					X				X													Pm
SD	EBT-45	P		S	mod.	mod.	575	120	30	C	A							X		X	O	R	R	R					X			Pm
SD	EBT-46				low	mod.	560	160	45	A	A									X		R	R	R	X		R		X			Pm/S
TN	EBT-62	P	S	S	low	mod.	35	10	5	A	C	C		C										C	X							Pm
MH	BIT-42	P	F	S	low	poor	140	35	4	A	C													C			X					Pm
DW	BIT-288	P	F	S	mod.	poor	190	60	5	C	C			X								R		R	X		R		X			Pl/Pm

Notes: Modal abundances are represented as: P=prevalent (50–100%), F=frequent (20–50%), and S=scarce (0≤20%). Relative abundances: A=abundant, C=common, O=occasional, R=rare, X=present, but abundance not estimated. Eruption type: Pm=phreatomagmatic, S=Strombolian, Pl=Plinian. In the case of mixed tephra the dominant eruption mode is listed first and the subsidiary mode second.

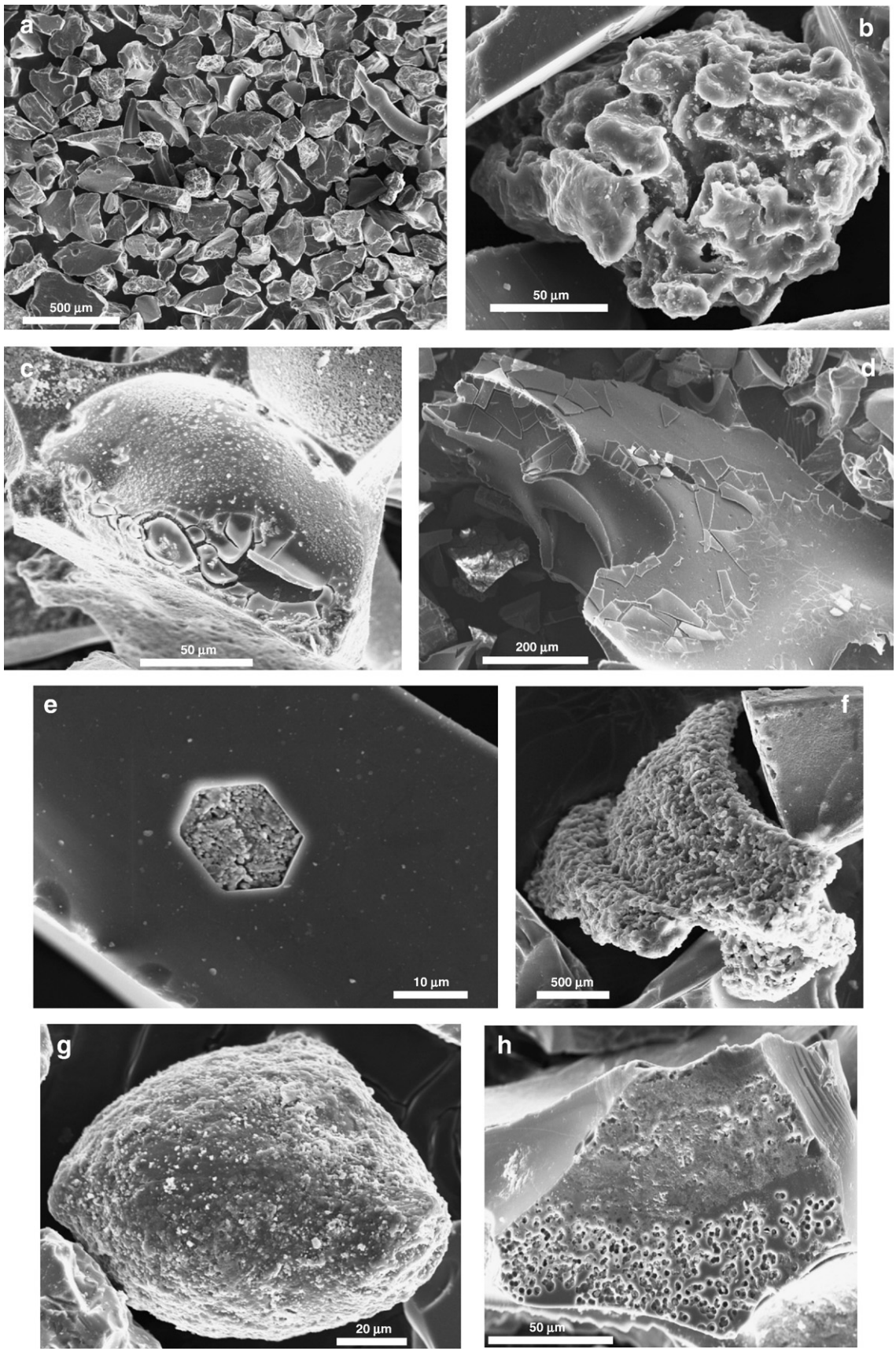

Fig. 3. Typical phreatomagmatic tephra and shard morphologies. (a) Typical phreatomagmatic end-member tephra (UB7). Note the abundance of blocky and platy low-vesicularity glass shards, some of which also display hackle marks. Where vesicles are present they have been truncated. (b) Mossy shard from tephra UB7, this shard is also shown in (a). (c) Typical hydration rind and sublimate coating on a shard from tephra SD2. (d) Turbulent shedding clearly demonstrated on a shard from the modern tephra sample. The cracking is only surficial and has resulted in flaking of the surface of the shard. (e) Sublimate and ash filled cavity of a glass shard from tephra UB27. The cavity was formed by the plucking of a phenocryst (likely apatite) from the shard. (f) Sublimate coated shard in tephra UB8. (g) An agglomeration of dust that is possibly an accretionary lapilli in tephra UB3. (h) An acid pitted surface on a shard from tephra UB3.

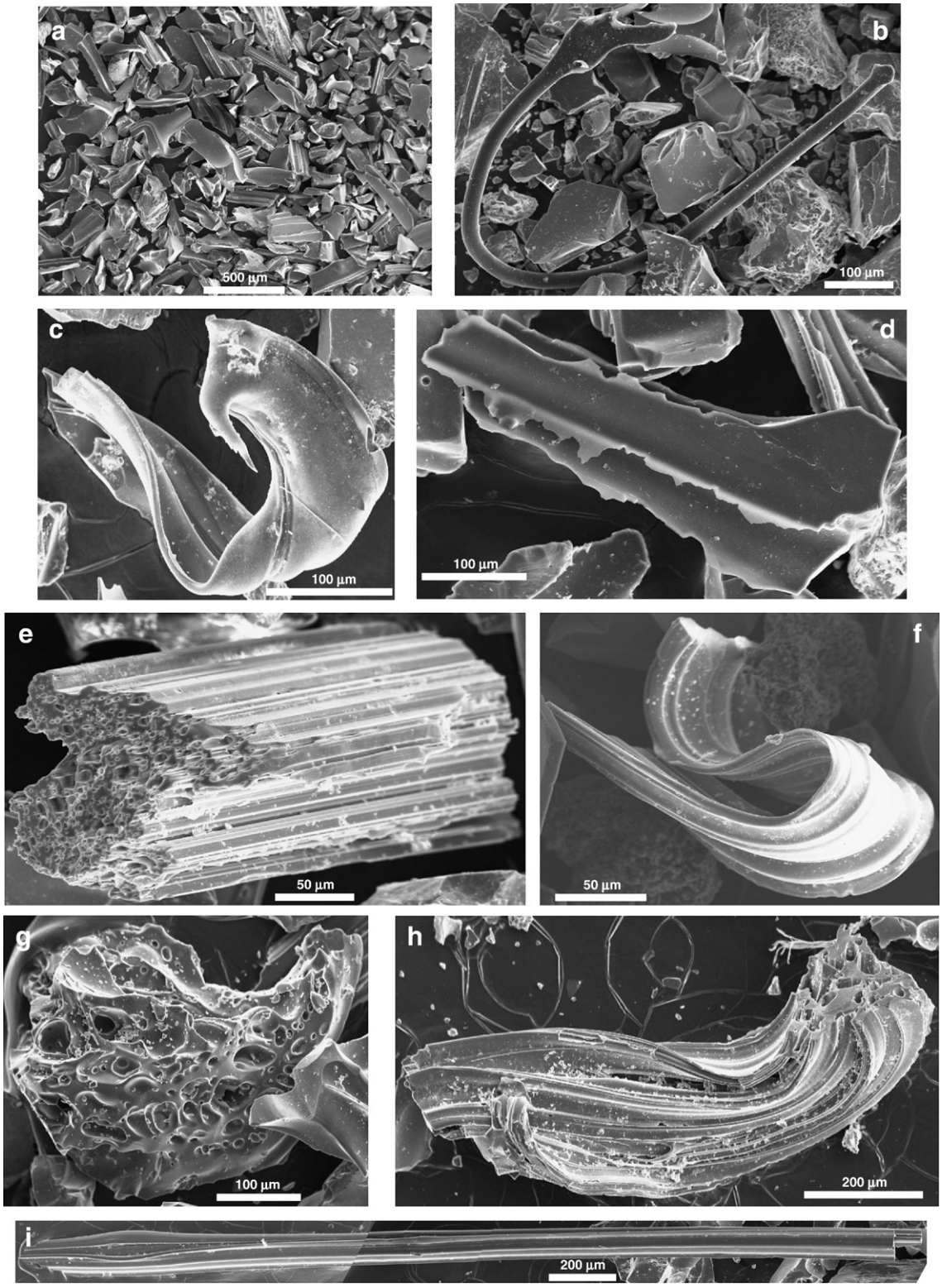

Fig. 4. Typical Strombolian tephra and shard morphologies. (a) Tephra UB23, which represents an end-member Strombolian tephra. (b) Pele's hair in tephra UB21. (c) Fluidal shard from tephra SD1. (d) Shard from tephra UB11 with torn and ragged edges where fragmentation has been caused by bubbles bursting and the fluidal forms of some of the clasts. (e) Typical pumice shard from tephra UB6. (f) Fluidal glass ribbon from tephra MB4. (g) Fluidal and highly vesiculated shard from tephra UB25. (h) Pumice shard from tephra LB7 that has been deformed and twisted. (i) Elongate glass shard from tephra LB7. The shard is not cylindrical rather it is ribbed and has small bulges that are likely the locations of unruptured vesicles.

that tephra shards are fragmented by brittle fracture rather than bubble expansion in phreatomagmatic eruptions. Group one tephra exhibit many typical phreatomagmatic shard morphologies. Wohletz (1983) and Heiken and Wohletz (1985) have shown that morphologies commonly observed in the tephra, such as blocky, platy, hackled, and mossy, are indicative of phreatomagmatic eruptions (Fig. 3). They have also noted many other commonly observed features like acid pitting, hydration rinds, and sublimate coatings in phreatomagmatic tephra (Fig. 3). Büttner et al. (1999) further observe that step-fractures (Fig. 3a) and quench cracks are found in both experimental and

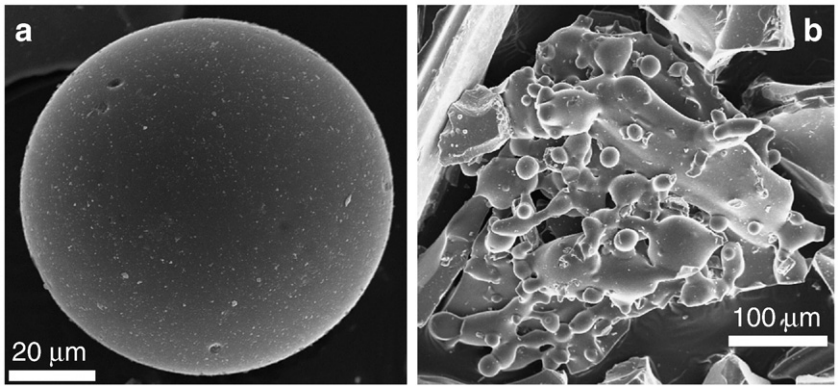

Fig. 5. Shards exhibiting spherical (a) and budding (b) morphologies from tephra UB20 and tephra UB25, respectively.

natural phreatomagmatic tephra. Mastin (2007) proposes that turbulent shedding, a process related to phreatomagmatic eruptions, results in clasts with thin skins that appear to be peeling off (Fig. 3d). All of these morphologies are observed in the tephra we interpret as phreatomagmatic. Heiken and Wohletz (1985) proposed that other features present such as dust coatings, dust-filled vesicles and cavities (Fig. 3e), and small accretionary lapilli-like aggregates (Fig. 3g) are also good indicators of phreatomagmatism. However, it is possible that these dust features formed during extraction of the tephra from the glacial ice and the consequent drying, thus, caution must be employed in their interpretation.

Group two tephra display many morphologies typical of Strombolian eruptions. Specifically, fluidal and deformed shards (Fig. 4), such as those observed by Walker and Croasdale (1971) and Heiken (1978) are abundant. Pumice, Pele's hair and torn shards (Fig. 4) are not typically reported for Strombolian eruptions. Duffield et al. (1977) report that Pele's hair is typically associated with Hawaiian style basalt eruptions. Nonetheless, Kyle (1977) reports that Pele's hair are often formed from small Strombolian eruptions at Erebus and that many of the bombs erupted during these eruptions have thread-like stringers and contain interior cavities crossed with abundant fine hairs. When these stringers and fine hairs are broken loose from their parent bombs they form Pele's hair. Rose (1987) observed morphologically similar Pele's hair formed by Strombolian eruptions at Stromboli volcano. Moune et al. (2007) have also documented Pele's hair from Strombolian eruptions at Masaya volcano. Heiken and Wohletz (1985) typically associate pumice with Plinian eruptions but Mangan and Cashman (1996) have also described high-vesicularity scoria clasts from fire fountains at Kilauea. Modern Strombolian bombs from Erebus are also highly vesiculated and often show signs of stretching and twisting similar to the pumice observed in the tephra samples (Kyle, 1977). The

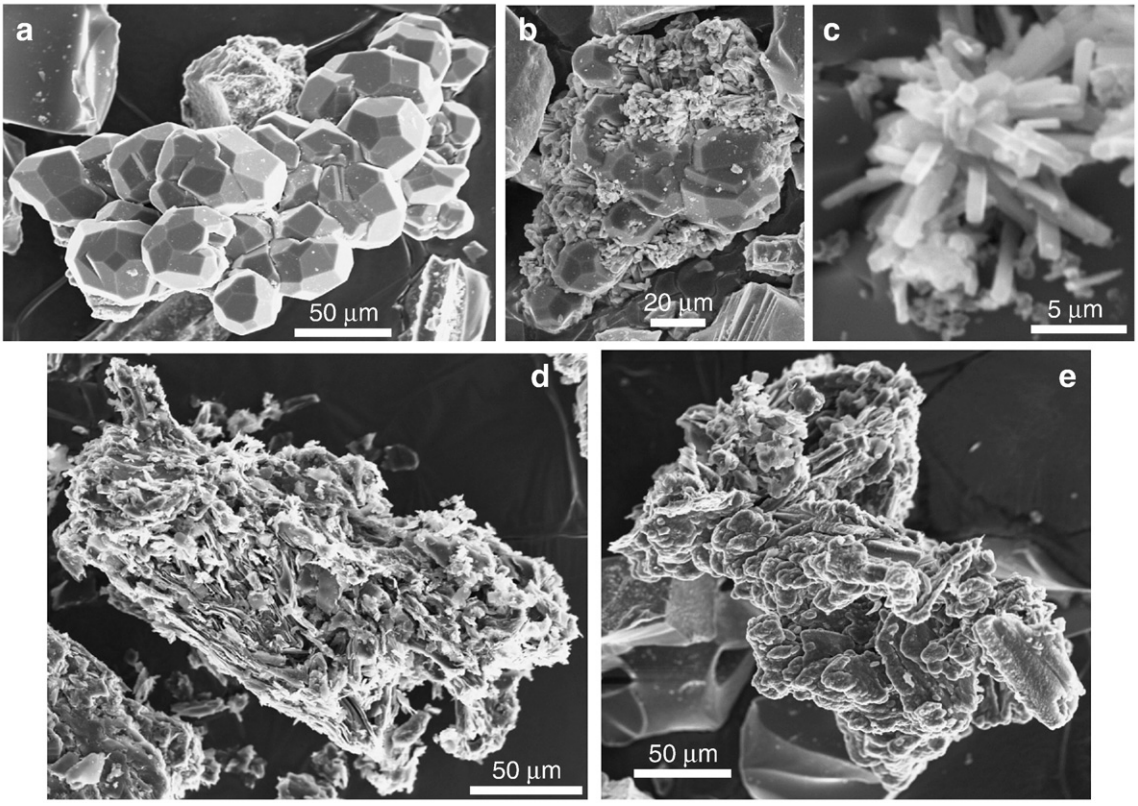

Fig. 6. Xenocrystic minerals from pre-eruption hydrothermal system. (a) Typical cluster of analcime crystals from tephra MB4. (b) An analcime cluster with intergrown zeolites from tephra MB4. (c) Zeolites, probably natrolite, on an analcime crystal from tephra UB21. (d) Undifferentiated clay minerals from tephra MB4. (e) Undifferentiated clay and zeolites from tephra MB4.

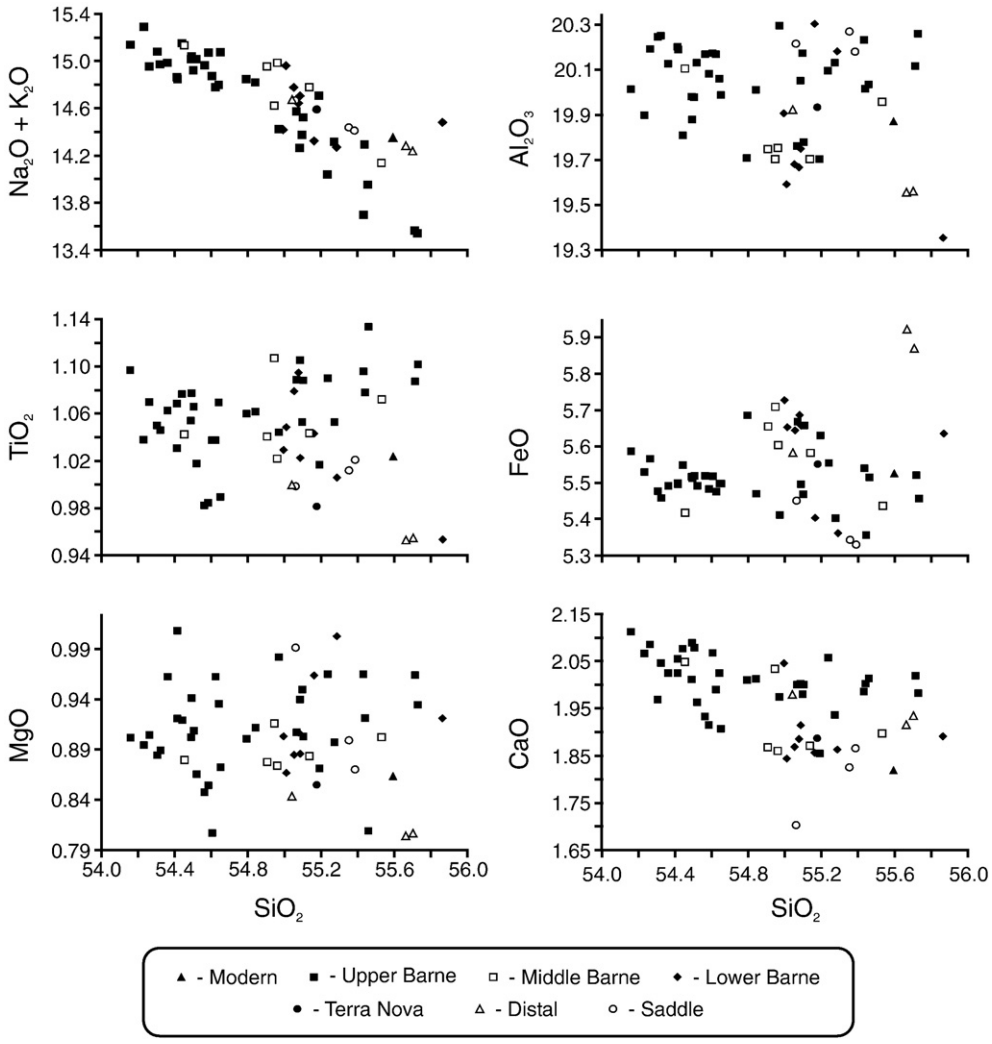

Fig. 7. Harker diagrams of major element geochemistry of glass shards showing that the geochemistry of the tephra is overall relatively homogeneous. Note that the upper left plot is a TAS diagram indicating that the tephra are all phonolite (after Le Bas et al., 1986).

pumice observed in the Strombolian tephra is therefore, most likely formed by these processes.

A significant number of the samples contain tephra typical of both Strombolian and phreatomagmatic eruptions. Panter and Winter (2008-this volume) also observe this in a thick, coarse tephra layer draping the rim of the Side Crater of Erebus. The combination of these two eruptive mechanisms is not unusual as many eruptions beginning with phreatomagmatic activity transition into magmatic activity as the water source is depleted. This progression was observed during eruptions of Surtsey (Thorarinsson, 1966), Capelinhos (Walker and Croasdale, 1971), and Ukinrek Maars (Self et al., 1980). Closely related phreatomagmatic and Strombolian activity has been reported at White Island (Houghton and Nairn, 1991) and interpreted from the deposits of Rothenberg scoria cone (Houghton and Schmincke, 1989). Dellino and La Volpe (1996) and Dellino and Liotino (2002) also encountered deposits from closely related magmatic and phreatomagmatic activity at Lipari related to the Monte Pilato-Rocche Rosse eruptions. The difference with these eruptions is that they all have abundant seawater or ground water available during the eruptions. The only water sources available for eruptions at Erebus volcano are snow and ice and possibly subsidiary water in a hydrothermal system derived from the percolation of melted snow and ice into the edifice. Several observed eruptions indicate that it is possible for snow and ice to affect a Strombolian eruption or cause interspersed phreatomagmatic activity. During the 1971 eruption of Mount Etna, discrete phreatomagmatic bursts caused by melt-water from snow and ice interacting with the magma were observed during a Strombolian rift eruption (Rittmann, 1971; as reported in Heiken and Wohletz, 1985, p. 44–45). Significant phreatomagmatic activity also occurred during the predominantly Strombolian 17–19 May 1994 eruption of Llaima volcano (Moreno R. and Fuentealba C., 1994).

Rowe et al. (2005) report another method for producing mixed eruptions that was observed at Erebus volcano, although it requires rather specific circumstances. On 19 December 1997 an avalanche of rock, snow and ice collapsed from the crater wall into the lava lake. Within a short time the lava lake started having small bubble burst eruptions, presumably due to snow and ice vaporizing. These events continued for 3 days and resulted in over 630 distinct eruptions, which produced identifiable seismic events. Although the response of the lava lake was small Strombolian eruptions there was a phreatomagmatic component. Only minor tephra were produced in the observed eruptions but if a larger collapse of snow and ice were to occur it would likely produce a more widely dispersed tephra showing mixed character.

Multiple eruption modes recorded in a single sample may also result from combining the tephra from several eruptions to form a single tephra layer. For example, tephra UB27 contains both phreatomagmatic and Strombolian ash and was collected from a broad diffuse layer that may contain two tephra units deposited from discrete eruptions. If these are independent tephra units, they were

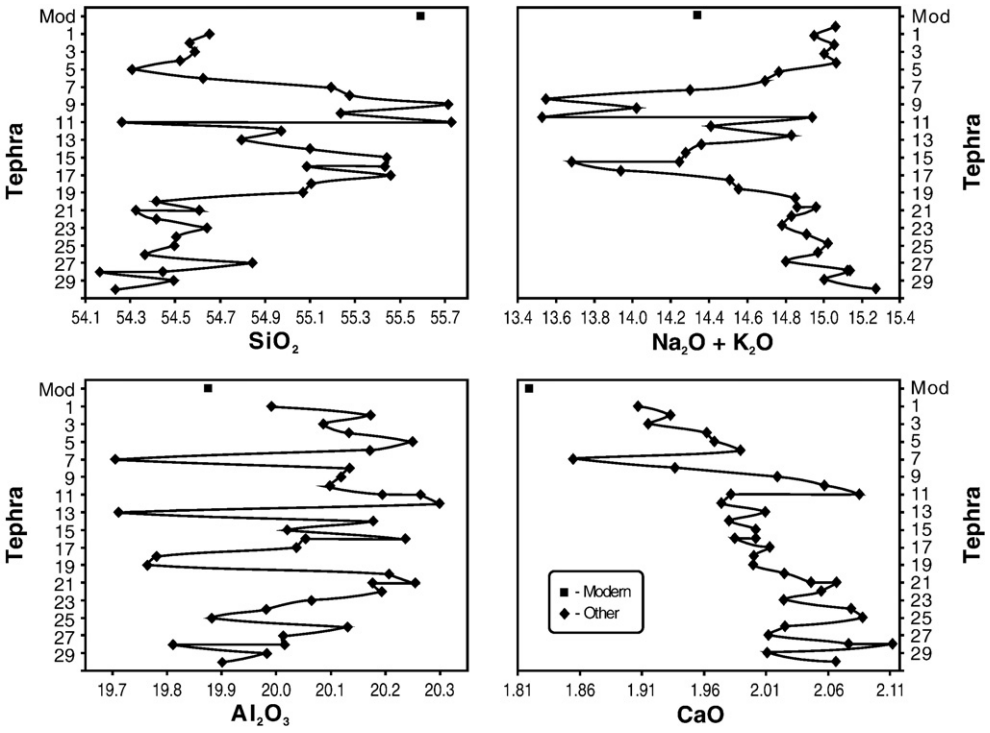

Fig. 8. Selected oxide concentrations of tephra from the modern tephra and Upper Barne site plotted against stratigraphic position. The numbers on the *y*-axis correspond to the number of the tephra layer at the Upper Barne site (1 corresponds to tephra UB1) and Mod refers to the modern tephra. Note that the trends apparent in the plots appear to be continued in the geochemistry of the modern tephra. Distance separating the tephra samples in the plots does not indicate the actual distance between tephra layers, rather the tephra have been arbitrarily plotted equidistant from each other.

likely deposited over a relatively short time span, perhaps several months and may be derived from the same batch of magma.

The distal tephra samples present several enigmatic circumstances. Both the Manhaul Bay and Mt. DeWitt tephra have grain sizes that are only slightly finer (average ~30 μm and ~60 μm, respectively) than the proximal tephra samples (average ~90–260 μm) and both have anorthoclase contents that are significantly higher than the proximal tephra (Fig. 10). An extremely powerful eruption must have occurred for relatively coarse tephra containing a significant crystal component to be deposited so far from the source. All of the anorthoclase analyzed from the distal tephra samples plot well within typical values for Erebus and are geochemically identical to anorthoclase in the proximal samples indicating that the high feldspar content is not a result of post-depositional contamination (Fig. 11).

The Manhaul Bay tephra is composed of platy and subordinate blocky shards and abundant anorthoclase. These shards indicate a phreatomagmatic origin yet the distal location, grain size, and abundant anorthoclase all indicate an unusually powerful eruption. Self and Sparks (1978) proposed that phreatoplinian eruptions are as powerful as Plinian eruptions. However, the cases studied by Self and Sparks (1978) involved large rhyolitic eruptions through caldera lakes, conditions that are not possible at Erebus due to the below-freezing ambient temperatures and phonolitic melt composition. Nonetheless, Simkin and Howard (1970), Naranjo S. et al. (1993), and Dellino and Kyriakopolous (2003) have documented phreatomagmatic eruptions of non-rhyolitic compositions that dispersed tephra over long distances. The composition of glass in the Manhaul Bay tephra is very similar to the proximal tephra. Therefore, the enhanced power of the Manhaul Bay eruption cannot be explained by a geochemical difference but is potentially found in the water source for the eruption. Begét et al. (1996) proposed that eruptions caused by magma interaction with permafrost and ice are more explosive because the thermal properties of the ice result in low water to melt ratios. Thus, phreatomagmatism caused by magma interaction with a large volume of snow or ice accumulated in and around the vent area could potentially have resulted in powerful eruptions. This effect could be augmented if the mass eruption rate was higher than the eruptions that produced the proximal tephra. The 8–9 August 1991 eruption of Hudson Volcano may provide an interesting corollary to the eruption

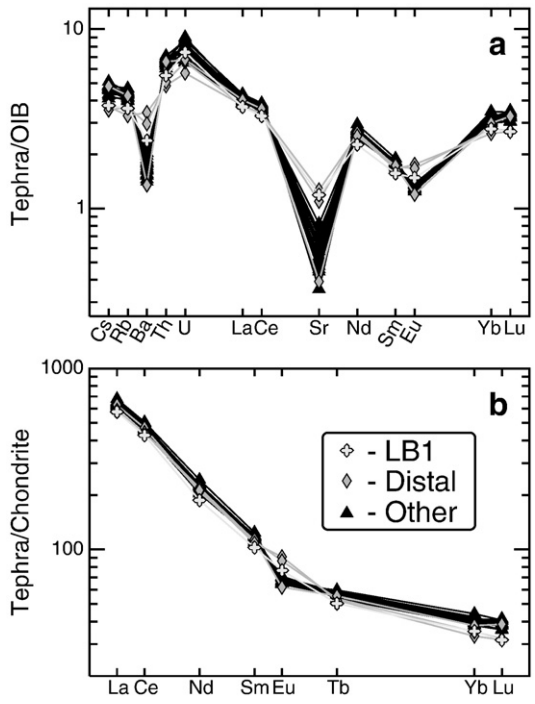

Fig. 9. OIB (a) and chondrite (b) normalized (Sun and McDonough, 1989) spider diagrams of whole tephra samples. Note the overall homogeneity of the compositions with the exception of Eu in (b) and Ba and Sr in (a), where wide variations corresponding to feldspar concentration exist. The distal tephra and tephra LB1 consistently have higher concentrations of the feldspar compatible elements.

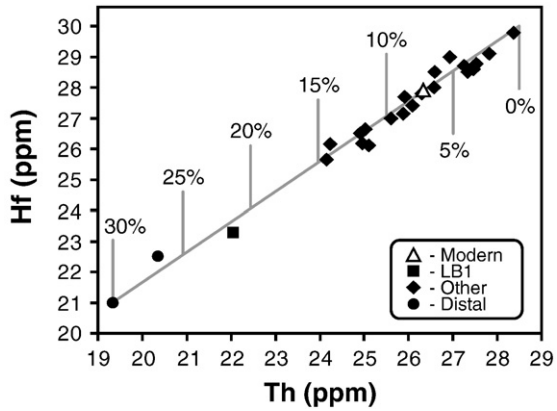

Fig. 10. Trace element variation diagram of Hf and Th concentrations of the bulk tephra samples. The observed trend is controlled by the feldspar content of the tephra, which can be calculated from the graph using a simple dilution model. The glass contains ~30 ppm Hf and ~28.5 ppm Th (Caldwell and Kyle, 1994), whereas the feldspar contains neither of these two elements. The line and percentages plotted in the graph indicates the calculated percentage of feldspar in the sample. This calculated value corresponds well with optically estimated feldspar contents. Note that the two distal tephra samples and tephra LB1 all have extremely high feldspar concentrations, but that typically the tephra have between ~2 and 15% feldspar.

that we propose formed the Manhaul Bay tephra. Naranjo S. et al. (1993) report that a basaltic fissure eruption in an ice-filled caldera resulted in enhanced phreatomagmatic activity that deposited up to 0.5 cm of tephra up to 200 km away from the volcano. Eruption power was likely further enhanced by the high anorthoclase content (~30%; Fig. 10), which is the highest of any of the tephra collected. The shards in the Manhaul Bay tephra also have abundant chipped edges indicating that the tephra has been subject to post-depositional wind transport.

The Mt. DeWitt tephra contains predominantly bubble wall fragments, platy shards, and occasional pumice. This morphology indicates that the eruption was dominantly Plinian but likely had a phreatomagmatic component. The eruption was likely more powerful due to the presence of water in the system but was also enhanced due to increased magma viscosity resulting from the relatively high SiO_2 concentration and phenocryst content (~27%, Fig. 10) of the Mt. DeWitt tephra. This potentially important phreatomagmatic component is further indicated when the tephra is compared to a Plinian phonolitic tephra. van den Bogaard and Schmincke (1985) and Juvigné et al. (1995) report that tephra from the 12.9 ka eruption of Laacher See volcano collected at approximately the same distance from source has a similar grain size to the Mt. DeWitt tephra but is composed exclusively of pumice shards. Thus for a melt of similar viscosity a Plinian eruption should provide copious pumice shards. However, Cioni et al. (1992), Naranjo S. et al. (1993), Rolandi et al. (1993), Bitschene and Fernandez (1995) and Dellino and Kyriakopolous (2003) have all reported phreatomagmatic components in the Plinian and subplinian eruptions of Etna on 26 October 2002, Hudson on 13 August 1991, and the 79 A.D. and 1631 eruptions of Vesuvius. All of these eruptions produced significant amounts of shards exhibiting phreatomagmatic morphologies. The Mt. DeWitt tephra was therefore likely to have formed in a Plinian eruption that had a phreatomagmatic component. The source of the water during this Plinian eruption was probably snow, ice, and the hydrothermal system of the volcano.

Erebus volcano has 2 calderas that form the rim of the summit plateau of the volcano. The Mt. DeWitt tephra has an age of 39±6 ka which places it within the inferred age range for the formation of the older caldera. It is possible that caldera collapse and the eruption of the Plinian tephra are related (Harpel et al., 2004). The bulk composition of the Mt. DeWitt tephra is tephriphonolite when the phonolitic glass and anorthoclase are mixed together. This composition is similar to the older, tephriphonolite pre-caldera lava flows in the summit area (Kyle et al., 1992; Harpel et al., 2004; Kelly et al., 2008b-this volume). The Manhaul Bay tephra remains undated but a phonolite whole rock composition is calculated when adjusted for anorthoclase content. The transition from tephriphonolite to phonolite compositions occurred about 36 ka (Harpel et al., 2004). Therefore the Manhaul Bay tephra is probably <36 ka, which places it within the age range for both caldera-forming events.

Vigorous phreatomagmatic eruptions were associated with caldera collapse during the 1968 Fernandina eruption (Simkin and Howard, 1970). Mastin (1997) examined the Keanakako'i Ash at Kilauea volcano and considers phreatomagmatic activity to have also been important in this caldera-forming eruption. However, in both of these instances pre-existing calderas were modified by subsidence of the caldera floor rather than the formation of a new caldera. It is possible that the Manhaul Bay tephra is associated with one of the caldera-forming events or an event that significantly modified a pre-existing caldera. Nonetheless, without better age constraint on both caldera formation and the Manhaul Bay tephra it is impossible to definitively correlate either tephra with a caldera-forming event and the possibility of passive piecemeal collapse must still be considered.

The Dry Valleys region, which is ice free and is located directly between Erebus and the distal-blue ice localities should contain tephra from these eruptions. Marchant et al. (1993, 1996) have described numerous tephra deposits in the Dry Valleys. However, up to 50 of these tephra have yielded ages in the millions to tens of millions of years range. Many of these tephra samples are phonolitic and contain abundant anorthoclase similar to Erebus tephra samples (Marchant et al., 1993). It is possible that some of the undated tephra samples from the Dry Valleys are related to eruptions at Erebus and may correlate to the distal tephra samples from this study.

The eruptions that produced the proximal tephra layers were likely small in size, depositing ash only locally. Ash has recently been found on Fang Glacier and was also reported by Keys et al. (1977) in the same locality. Nonetheless, Kyle et al. (1982) do not report any eruptions during the last 35 years of observation, even during periods of enhanced eruptive activity, that have produced tephra in the volumes implied by the englacial tephra layers. Therefore, the eruptions that produced the proximal tephra were comparatively large Strombolian and phreatomagmatic events, but were regionally insignificant. The observed activity at Erebus also implies that many small eruptions have likely occurred throughout the life of the volcano but have not produced tephra deposits.

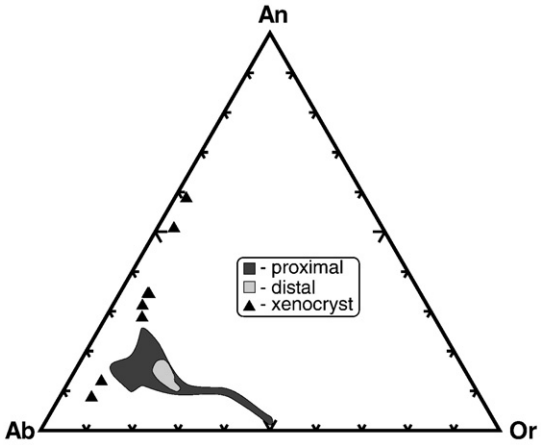

Fig. 11. Compositions of feldspar phenocrysts from the tephra samples. The narrow extension of the proximal compositions toward the orthoclase end member is caused by a single sanidine that is within the observed variation of modern juvenile feldspar from Erebus (Kyle et al., 1992). Note also that the feldspar from the distal tephra plot within the range of juvenile compositions. Only eight of the 200 feldspar analyzed are considered to be xenocrystic. Analytical details of the electron microprobe analysis of feldspar are identical to those reported in the notes to Table 1 with the exception that feldspar was analyzed using a 10 μm beam and a beam current of 20 nA.

6.2. Spherical and budding shards

Droplets and budding ash occur in some tephra samples (Table 3; Fig. 5). Spherical droplets have been reported in tephra of diverse geochemical compositions but only rare droplets have been reported with more silicic compositions such as andesite and phonolitic-trachyte (Hay et al., 1979; King and Wagstaff, 1980). Rose and Hoffman (1982) report that coal-fly ash, which are small, spherical droplets, can also contaminate volcanic ash. Coal-fly ash contamination is not a possible source for the droplets in this study because of the isolation of Antarctica from man-made pollutants and the pre-industrial age of the majority of tephra layers.

Single spheres are reported in the plumes of passively degassing shallow (on the scale of meters) magma at St. Augustine volcano (Cadle and Mroz, 1978; Hobbs et al., 1978), Mount Etna (Lefèvre et al., 1986, 1991; Spadaro et al., 2002) and Kilauea (Lefèvre et al., 1991; Meeker and Hinkley, 1993). These spheres were formed from a very fine magmatic mist caused by the bursting of bubbles during passive degassing. Degassing of the Erebus lava lake should provide the appropriate conditions for the formation of glass spheres. Glass spheres have not been observed during aerosol sampling of the Erebus plume (Chuan et al., 1986; Chuan, 1994). Thus, it is unlikely that passive degassing formed the observed spheres. The association of the observed droplets with tephra layers is also strong circumstantial evidence of an eruptive origin.

Many researchers have noted droplets in the deposits from phreatomagmatic explosions in low-viscosity basaltic or experimental settings (Heiken and Lofgren, 1971; Wohletz, 1983; Wohletz and McQueen, 1984; Zimanowski et al., 1986, 1997). Zimanowski et al. (1997) produced droplets, fluidal shards, and Pele's hair in experimental phreatomagmatic explosions and found that the quantity of such shards was proportional to acceleration rate and ejection speed. In general, dry conditions, i.e. low water to melt ratios, during a phreatomagmatic eruption are also considered to produce more vigorous eruptions and would yield the appropriate conditions to form droplets (Wohletz, 1983; Zimanowski et al., 1997; Büttner and Zimanowski, 1998; Morrissey et al., 2000). Begét et al. (1996) further propose that magma interaction with the ice in permafrost will cause very low water to melt conditions and enhance

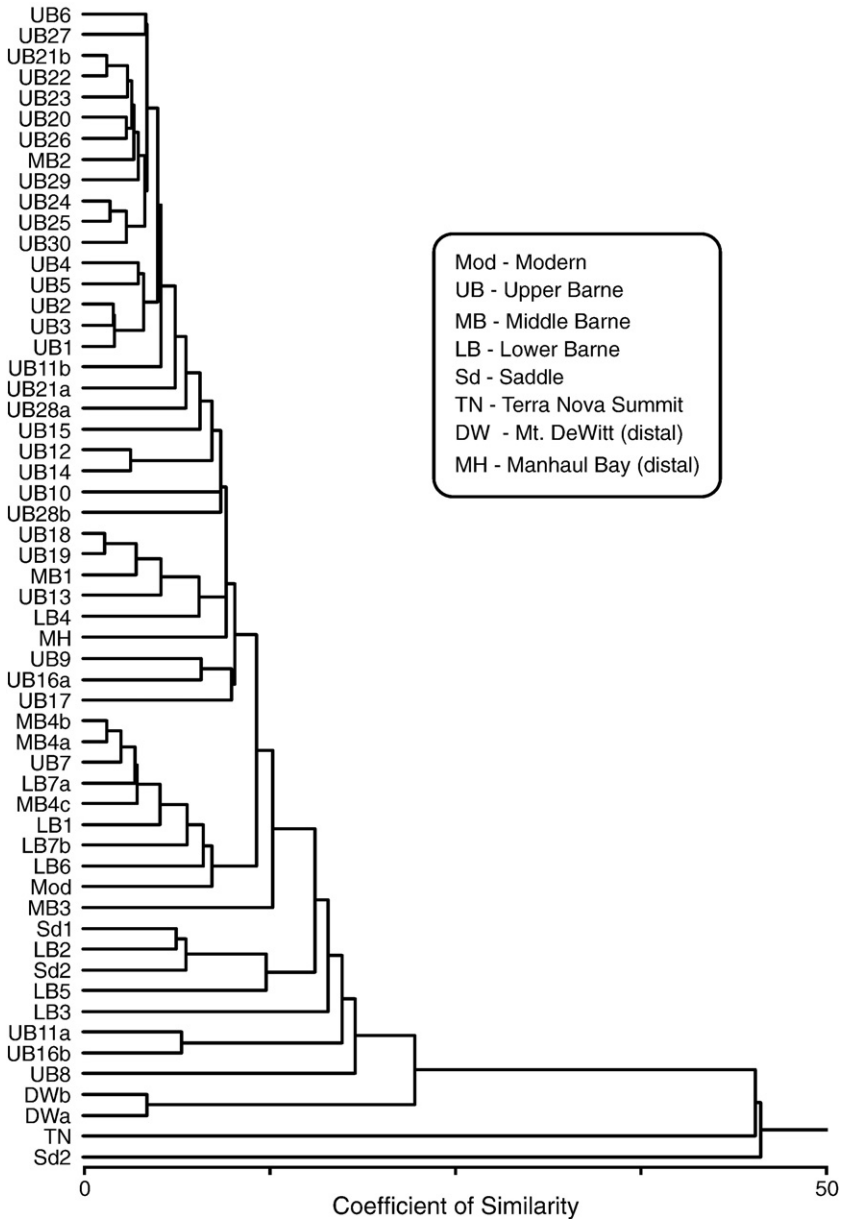

Fig. 12. Dendrogram generated from the D^2 matrix using the nearest neighbor method. The Upper Barne tephra have formed a broad cluster and to a more limited extent some stratigraphic clustering is present.

explosivity. Thus, if the melt at Erebus interacted with snow or ice, as is likely, this would cause low water to melt ratios and highly vigorous phreatomagmatic eruptions that would yield droplets.

Spheres have also been noted in deposits from fire fountaining at Kilauea (Baker, 1968; Heiken and Lofgren, 1971; Heiken, 1972; Duffield et al., 1977; Lefèvre et al., 1991), Etna (Lefèvre et al., 1986, 1991), and in lunar eruptions (Heiken and Lofgren, 1971; Heiken and Wohletz, 1985). Fire fountaining, however, has never been observed at Erebus and no spatter or reticulite deposits indicative of such activity are known. Heiken and Wohletz (1985) report that fluidal shards are commonly observed in Strombolian tephra. Moune et al. (2007) also report spheres in the tephra from Strombolian eruptions of Masaya volcano. Therefore, the droplets in the Erebus tephra samples must have been formed during both phreatomagmatic and Strombolian eruptions.

Budding ash (Fig. 5b) is found in only six of the samples, two derived from purely phreatomagmatic tephra and four from mixed tephra with a strong Strombolian component. The examples from the phreatomagmatic tephra are poorly developed, whereas the best examples come from the mixed tephra. Hay et al. (1979) describe similar clasts occasionally found in the trachytic Mount Suswa globule ignimbrite and Tallmadge (1978) also experimentally produced similar-looking clasts from a steel melt. Budding ash represents melt globules that have been quenched during either disaggregation or coalescence and is likely related to the spheres. To form spheres a globule of melt must hydrodynamically split off from a parent globule and remain liquid long enough for surface tension to form the sphere. Coalescence requires that the droplet remain liquid long enough for at least two droplets to contact each other and surface tension to be overcome allowing the droplets to merge. Heiken and Lofgren (1971) observed that coalescence of droplets appears to be rare in natural low-viscosity melts. Furthermore, Yule and Dunkley (1994, p. 22) note that in metal melts coalescence is retarded by the high surface tensions, which Liu (2000, p. 78, 80) reports range in values from ~0.378–1.873 Pa·m (Pascal meters). Comparatively, the surface tension for a Hawaiian basalt is ~0.3 Pa·m (Mastin, 2007). Assuming that basalt and phonolite melts have similar surface tension values it is likely that coalescence would be retarded in Erebus melts as with the metal melts. Thus, it seems unlikely that coalescence played an important role in the formation of the budding ash. Tallmadge (1978) reached the same conclusion regarding the generation of his similar-shaped particles.

Quenching during disaggregation of a globule is the most likely mode of formation for budding ash. Yule and Dunkley (1994, p. 38) note that premature quenching of an industrial melt prior to droplet formation will result in misshapen particles and that this is especially prevalent in interactions between water and melt. Thus, the presence of these droplets in phreatomagmatic and mixed tephra deposits is not surprising.

The budding shard morphology is not widely reported in other natural settings nor is it noted in all of the Erebus tephra. Yule and Dunkley (1994, p. 27) report that in relatively high-viscosity glass, ceramic, and polymer melts, viscosity is the main factor retarding droplet formation. Thus, the moderate viscosity of the Erebus phonolite melt might explain the presence of budding ash. Melt viscosities calculated using the methods of Shaw (1972) and Giordano and Dingwell (2003), a temperature of 1000 °C (a typical eruptive temperature; Kyle et al., 1982), glass compositions from this study, and 0.15% H_2O (Dunbar et al., 1994) are 10^3 Pa·s. Carmichael et al. (1974, p. 145) also calculated a viscosity of 10^3 Pa·s for Erebus phonolite at 1000 °C using the method of Bottinga and Weill (1972). Similarly, Hay et al. (1979) calculate viscosities ranging from 10^2–10^5 Pa·s for a trachyte roughly analogous to the Erebus phonolite. Comparatively, Shaw et al. (1968) and Moore (1987) report viscosities as low as 50–100 Pa·s for Hawaiian basalts. It is possible that the viscosity of the basalts is low enough that they can disaggregate completely before quenching occurs. Whereas the Erebus phonolite has a low enough viscosity to form occasional droplets but is high enough that shards can be quenched prior to droplets completely splitting off, forming budding tephra. Nonetheless, fragmentation is an extremely complicated process (Yule and Dunkley, 1994; Cashman et al., 2000; Morrissey et al., 2000) and it is possible that conditions conducive to droplet formation might exist locally within an eruption regardless of melt viscosity. The phreatomagmatic nature of the eruptions may have also contributed to the preservation of the budding morphology by enhancing the quench rate or producing localized areas that are quenched more rapidly than other areas.

6.3. Analcime and other zeolites

The analcime present in some of the samples is likely a xenocrystic phase. Heiken and Wohletz (1985) have observed analcime in tephra from Coliseum Diatreme in the Hopi Buttes volcanic field and Heiken (1972, 1974), and Heiken and Wohletz (1985) report nepheline (closely related to analcime) in tephra samples from Ol Doniyo Lengai volcano. However, in both locations the crystals are heavily covered in sublimate and or glass and have poor crystal form. The analcime crystals in this study have excellent crystal form with no adhering glass, embayment, resorption, or other signs of contact with the pre-eruption magma, making it unlikely that they are a juvenile crystal phase. de'Gennaro et al. (2000) report a similar assemblage of analcime and other zeolites in the Neapolitan Yellow Tuff that formed in situ after deposition due to the long cooling time and abundant water within the pyroclastic flow deposits. However, the size of the Erebus tephra dictates that they were deposited cold (Thomas and Sparks, 1992). Thus, the undifferentiated zeolites and analcime must have formed prior to or within the first few seconds of the eruption. However, the analcime crystals are too large to have formed by vapor phase crystallization during an eruption. Small, rare zeolites adhering to juvenile glass shards in several of the tephra samples indicate that some zeolites were probably formed in the very early seconds of the eruption. However, most of the zeolites are not associated with juvenile clasts. Jakobsson and Moore (1986) report morphologically identical analcime crystals as a common phase in the hydrothermal system at Surtsey volcano and zeolites in general are a very common species within hydrothermal systems. Clay is also highly suggestive of the existence of a hydrothermal system (Ohba and Nakagawa, 2002). The most logical explanation for the presence of clay, analcime and most of the zeolites in the tephra samples is that they are xenocrysts incorporated into the tephra from a pre-eruption hydrothermal system. Ohba and Nakagawa (2002) have documented that entrainment of xenocrysts from hydrothermal systems is not an uncommon process during eruptions. This hypothesis is also supported by the observation that these phases are found in purely Strombolian tephra. Typically sublimation is only associated with phreatomagmatic eruptions and for analcime, a hydrous phase, to form abundant water must be present.

7. Geochemistry

7.1. Geochemical correlation

The Euclidean distance (D, but typically values are expressed as D^2, the square of the Euclidean distance), measured in units of standard deviation, is used to compare major element and Cl concentrations for each sample. This method is commonly used to compare the similarity between individuals within a population (see Davis, 2002, p. 477). Perkins et al. (1995, 1998) used this method to correlate tephra but found that it was necessary to account for the varying analytical precision between oxides and the number of shard analyses averaged to obtain the final tephra composition. However, the method of Perkins et al. (1995, 1998) does not yield statistically identical D^2 values for the pairs of tephra known to be identical in this data set. Therefore, when calculating the Euclidean distance the major element

concentrations were weighted according to the number of shards analyzed and the analytical precision for each oxide by using a simple weighted mean. Thus, the modified Euclidean distance was calculated using:

$$D^2 = \sum_{k=1}^{n} \left(\frac{(x_{k1} - x_{k2})^2}{\left(\frac{m_1\sigma_{k1}^2 + m_2\sigma_{k2}^2}{m_1 + m_2 - 2} \right)} \right)$$

where x_{k1} and x_{k2} are the concentrations of element k for tephra samples 1 and 2, m_1 and m_2 are the number of shards analyzed to obtain the average composition of tephra samples 1 and 2, and σ_{k1} and σ_{k2} are the analytical precision for element k for tephra samples 1 and 2. For this study the analytical precision used for all of the samples is the same, thus $\sigma_{k1} = \sigma_{k2}$. Values of D^2 follow a χ^2 distribution with a D^2 value of zero indicating perfect correlation between two samples. Degrees of freedom are one less than the number of elements used for correlation. A degree of freedom is also lost due to the normalization of analyses to 100 wt.%. If 12 elements are used for correlation there are ten degrees of freedom and samples with $D^2 \leq 18.3$ are considered to be statistically identical at the 95% confidence level.

A total of 56 tephra samples were compared yielding 1540 possible correlations in the resulting matrix. Two samples each were taken from tephra layers LB7, UB11, UB16, UB21, UB28, and DW and three samples were taken from layer MB4. The comparisons between samples from the same tephra layers are known to be correlative. Values of D^2 range from 1.5 to 405.4 and yield a total of 252 pairs with D^2 values that are statistically identical. Seven of the 15 known correlative pairs yield D^2 values that are statistically identical. The number of correlations for each tephra sample ranges from 0–22 with an average of 9 correlative tephra for each tephra sample. Dendrograms developed using the nearest neighbor and centroid methods yielded nearly identical results. Some stratigraphically controlled clustering occurs on the dendrogram (Fig. 12) developed from the matrix of D^2 values, with seven of the first pairings and two of the second pairings occurring between tephra that are stratigraphically next to each other and a minor cluster occurring between tephra UB1–UB5. However, only two pairs, tephra MB4 and Mt. Dewitt, of the duplicate samples cluster together on the first pairing. On a more broad scale the majority of the tephra from the Upper Barne site cluster together and only have a single tephra, MB2, from another site included.

Three tephra layers (TN, UB8, and DW) are geochemically distinct from all of the other tephra samples. The Saddle tephra (Sd) were diffusely dispersed in firn and cannot be associated with a specific tephra layer or stratigraphic location. The two distal tephra layers do not have D^2 values indicating that they are statistically identical.

7.2. Geochemical considerations

The high degree of statistical correlation between the tephra samples indicates that the major element compositions of the tephra from Erebus volcano have been relatively homogeneous throughout the time period represented by the tephra. Microprobe analyses of glass in 27 lava bombs erupted from Erebus between 1972 and 2004 are identical within analytical error (Kelly et al., 2008b-this volume) and indistinguishable from most of the glasses analyzed here. This indicates that there is good potential of identifying Erebus as the source of an unknown tephra layer, but it will be difficult to correlate the tephra to an individual eruption or tephra layer from proximal locations on Mt. Erebus.

Alteration of clasts, especially through hydration and interaction with acid gases, is always a consideration when discussing geochemical trends of tephra formed during phreatomagmatic or Strombolian eruptions. For example, Spadaro et al. (2002) found extreme variation in the compositions of microspheres collected from Mt. Etna volcano that is attributed to the interaction of these clasts with acid gases. The observed variations of Spadaro et al. (2002) are over a larger compositional range than the trends we observe in the Erebus tephra. Moune et al. (2007) found similar compositional variation in shards from Masaya volcano. An added issue with the Erebus tephra is that they have been preserved in glacial ice for up to tens of thousands of years and could have been subjected to hydration during this period of time. The tephra samples typically contain pristine glass shards but signs of hydrous alteration, such as hydration rinds and acid etching, are noted. Nonetheless, we argue that large, alteration-induced compositional variations are not represented in our analyses of Erebus tephra. This is supported by the following observations. Few to no differences in clast density were noted in the backscattered electron imagery collected during electron microprobe analyses with the exception of rare, thin skins of alteration. These altered surfaces were avoided during microprobe analyses and should not affect the final compositions. In addition, totals from analyses of individual shards are within several percent of 100% indicating a low volatile content and hence little possibility of alteration. Low standard deviation values between analyses also indicate that intra-tephra clast compositions are also relatively homogeneous (Table 1). Furthermore, the geochemical trends that we observe are systematic within tephra layers separated by time intervals of possibly up to thousands of years. Any alteration-induced compositional differences would not systematically change over such a time span. From these observations we conclude that, though surficial alteration took place in some cases the geochemical compositions reported in Table 1 are representative of parent melt compositions and the geochemical trends within the tephra reflect changes in magma compositions over time.

Several lines of evidence lead to the conclusion that these tephra are all derived from Erebus volcano. The proximity of most of the tephra sites to Erebus is a strong argument that it is the source. Furthermore, the major and trace element geochemistry of all of the tephra are identical to the values by Kyle et al. (1992), Caldwell and Kyle (1994), and Kelly et al. (2008b-this volume) for Erebus volcano. Also, the Erebus tephra have an identical mineral assemblage and feldspar geochemistry to that reported by Kyle et al. (1992) for Erebus. Thus, all evidence indicates that Erebus is the source for these tephra.

Variations of glass compositions in tephra (Fig. 8) from the Upper Barne sequence indicate that the magma composition or its degree of crystallinity has varied subtly over the last ~33 ky (using the estimated timing of this sequence by Harpel et al., 2004). This is best marked by the decrease in CaO with time but there is also some systematic variation in SiO_2 content. Clearly over the time represented by the UB tephra there are systematic changes, which may be related to the magma production, evolution, and fractionation in the magmatic system.

The trace element compositions of the tephra are uniform with the exception of the feldspar-controlled elements. These trace element trends are typical of Erebus volcano and the McMurdo Volcanic Group in general (Kyle and Rankin, 1976; Sun and Hanson, 1976; Kyle, 1977; Kyle et al., 1992; Caldwell and Kyle, 1994; Kelly et al., 2008b-this volume).

8. Conclusions

Englacial tephra layers on the flanks of Mt. Erebus record at least 43 explosive eruptions. Phreatomagmatic eruptions have been prominent in the eruptive history of Erebus volcano and many tephra indicate they formed in mixed Strombolian and phreatomagmatic eruptions. Only a small number of tephra have a purely Strombolian eruption origin. Tephra was deposited onto the flanks of Mount Erebus and several nearby volcanoes. At least two large eruptions occurred that deposited tephra ~200 km from source. One was phreatomagmatic and is likely the result of magma interaction with snow and ice, the other was Plinian but with a phreatomagmatic component.

Spherical glass droplets present in some of the phonolitic tephra were formed during both phreatomagmatic and Strombolian eruptions. Ash with budding morphology represents the parent melt that has been quenched before these spheres could be hydrodynamically

split off. Small clusters of analcime crystals, other zeolites, and clay were formed in a pre-eruption hydrothermal system and then incorporated into the tephra as xenocrysts during the eruption.

All tephra analyzed have phonolitic glass compositions and contain a mineral assemblage of predominantly anorthoclase, with subsidiary apatite, olivine, Fe–Ti oxide, and sulfide phases. All of the phonolitic tephra are derived from Erebus volcano as indicated by mineralogy, major and trace element geochemistry, and feldspar geochemistry, and in many cases proximity to the volcano. The trace element geochemistry is homogeneous with the exception of feldspar-controlled compatible trace element concentrations. Several subtle trends in SiO_2 and CaO content are apparent in the glass compositions with stratigraphic position.

Acknowledgments

The authors extend their thanks to Al Eschenbacher, Kurt Panter, Lois Wardell, and Rich Esser who provided invaluable assistance in the field. The National Science Foundation contractor, Antarctic Support Associates, provided excellent logistical support. Petroleum Helicopters Inc. provided helicopter transportation without which this study would have been impossible. GPS support was provided by UNAVCO with specific thanks going to Oivind Ruud, Bjorn Johns, and Beth Bartel for help in the field and with data processing. Discussions with Richard Lefever on statistical analysis and correlation were extremely helpful during the preparation of this paper. Review and excellent comments by an anonymous reviewer were appreciated and review and conversations with Larry Mastin aided significantly in improving this manuscript. This work was supported through grants from the Office of Polar Programs, National Science Foundation.

References

Baker, G., 1968. Micro-forms of hay-silica glass and volcanic glass. Mineral. Mag. 36, 1012–1023.
Begét, J.E., Hopkins, D.M., Charron, S.D., 1996. The largest known maars on Earth, Seward Peninsula, northwest Alaska. Arctic 49, 62–69.
Bitschene, P.R., Fernandez, M.I., 1995. Volcanology and petrology of fallout ashes from the August 1991 eruption of the Hudson volcano (Patagonian Andes). In: Bitschene, P.R., Mendia, J. (Eds.), The August 1991 Eruption of the Hudson Volcano (Patagonian Andes): A Thousand Days After. Argentina, Comodoro Rivadavia, pp. 27–54.
Bottinga, Y., Weill, D.F., 1972. The viscosity of magmatic silicate liquids: a model for calculation. Am. J. Sci. 272, 438–475.
Büttner, R., Zimanowski, B., 1998. Physics of thermohydraulic explosions. Phys. Rev. 57, 5726–5729.
Büttner, R., Dellino, P., Zimanowski, B., 1999. Identifying magma–water interaction from the surface features of ash particles. Nature 401, 688–690.
Cadle, R.D., Mroz, E.J., 1978. Particles in the eruption cloud from St. Augustine volcano. Science 199, 455–456.
Caldwell, D.A., Kyle, P.R., 1994. Mineralogy and geochemistry of ejecta erupted from Mt. Erebus, Antarctica, between 1972 and 1986. In: Kyle, P.R. (Ed.), Volcanological and Environmental Studies of Mt. Erebus, Antarctica, Antarctic Research Series, vol. 66. American Geophysical Union, Washington DC, pp. 147–162.
Carmichael, I.S.E., Turner, F.J., Verhoogen, J., 1974. Igneous Petrology. McGraw-Hill International Series in the Earth and Planetary Sciences, New York.
Cashman, K.V., Sturtevant, B., Papale, P., Navon, O., 2000. Magmatic fragmentation. In: Sigurdsson, H., Houghton, B., McNutt, S.R., Rymer, H., Stix, J. (Eds.), Encyclopedia of Volcanoes. Academic Press, New York, pp. 421–430.
Chuan, R.L., 1994. Dispersal of volcano-derived particles from Mt. Erebus in the Antarctic atmosphere. In: Kyle, P.R. (Ed.), Volcanological and Environmental Studies of Mt. Erebus, Antarctica. Antarctic Research Series, vol. 66. American Geophysical Union, Washington DC, pp. 97–102.
Chuan, R.L., Palais, J.M., Rose, W.I., Kyle, P.R., 1986. Particle sizes and fluxes of the Mt. Erebus volcanic plume, December 1983. J. Atmos. Chem. 4, 467–477.
Cioni, R., Sbrana, A., Vecci, R., 1992. Morphologic features of juvenile pyroclasts from magmatic and phreatomagmatic deposits of Vesuvius. J. Volcanol. Geotherm. Res. 51, 61–78.
Davis, J.C., 2002. Statistics and Data Analysis in Geology. John Wiley & Sons, New York.
de'Gennaro, M., Cappelletti, P., Langella, A., Perrotta, A., Scarpati, C., 2000. Genesis of zeolites in the Neapolitan Yellow Tuff: geological, volcanological and mineralogical evidence. Cont. Min. Pet. 139, 17–35.
Dellino, P., Kyriakopolous, K., 2003. Phreatomagmatic ash from the ongoing eruption of Etna reaching the Greek island of Cefalonia. J. Volcanol. Geotherm. Res. 126, 341–345.
Dellino, P., La Volpe, L., 1996. Image processing analysis in reconstructing fragmentation and transportation mechanisms of pyroclastic deposits. The case of Monte Pilato–Rocche Rosse eruptions, Lipari Islands (Aeolian islands, Italy). J. Volcanol. Geotherm. Res. 71, 13–29.
Dellino, P., Liotino, G., 2002. The fractal and multifractal dimension of volcanic ash particles contour: a test study on the utility and volcanological relevance. J. Volcanol. Geotherm. Res. 113, 1–18.
Dellino, P., Isaia, R., La Volpe, L., Orsi, G., 2001. Statistical analysis of textural data from complex pyroclastic sequences: implications for fragmentation processes of the Agnano-Monte Spina Tephra (4.1 ka), Phlegraean Fields, southern Italy. Bull. Volcanol. 63, 443–461.
Dibble, R.R., Kienle, J., Kyle, P.R., Shibuya, K., 1984. Geophysical studies of Erebus volcano, Antarctica from 1974 December to 1982 January. N.Z. J. Geol. Geophys. 27, 425–455.
Dibble, R.R., Kyle, P.R., Skov, M.J., 1994. Volcanic activity and seismicity of Mt. Erebus 1986–1994. Antarc. J. U.S. 29, 11–14.
Duffield, W.A., Gibson Jr., E.K., Heiken, G., 1977. Some characteristics of Pele's hair. J. Res. U.S. Geol. Surv. 5, 93–101.
Dunbar, N.W., Cashman, K.V., Dupré, R., 1994. Crystallization processes of anorthoclase phenocrysts in the Mount Erebus magmatic system: evidence from crystal composition, crystal size distributions, and volatile contents of melt inclusions. In: Kyle, P.R. (Ed.), Volcanological and Environmental Studies of Mt. Erebus, Antarctica. Antarctic Research Series, vol. 66. American Geophysical Union, Washington DC, pp. 129–146.
Dunbar, N.W., Kyle, P.R., McIntosh, W.C., Esser, R.P., 1995. Geochemical Composition and Stratigraphy of Tephra Layers in Antarctic Blue Ice: Insights into Glacial Tephrochronology. VII International Symposium on Antarctic Earth Sciences, Sienna, Italy.
Esser, R.P., Kyle, P.R., McIntosh, W.C., 2004. $^{40}Ar/^{39}Ar$ dating of the eruptive history of Mt. Erebus, Antarctica: volcano evolution. Bull. Volcanol. 66, 671–686.
Gerst, A., Hort, M., Kyle, P.R., Voge, M., 2008. 4D velocity of Strombolian eruptions and man-made explosions derived from multiple Doppler radar instruments. J. Volcanol. Geotherm. Res. 177, 648–660 (this volume). doi:10.1016/j.jvolgeores.2008.05.022.
Giggenbach, W.F., Kyle, P.R., Lyon, G.L., 1973. Present volcanic activity on Mt. Erebus, Ross Island, Antarctica. Geology 1, 135–136.
Giordano, D., Dingwell, D.B., 2003. Viscosity of hydrous Etna basalt: implications for Plinian-style basaltic eruptions. Bull. Volcanol. 65, 8–14.
Hallett, R.B., Kyle, P.R., 1993. XRF and INAA determinations of major and trace elements in Geological Survey of Japan igneous and sedimentary rock standards. Geostand. Newsl. 17, 127–133.
Harpel, C.J., 2000. Late Quaternary eruptive history of Mount Erebus, Antarctica using $^{40}Ar/^{39}Ar$ geochronology and tephrostratigraphy. M.S. Thesis, Socorro, New Mexico Institute of Mining and Technology.
Harpel, C.J., Kyle, P.R., Esser, R.P., McIntosh, W.C., Caldwell, D.A., 2004. $^{40}Ar/^{39}Ar$ dating of the eruptive history of Mt. Erebus, Antarctica: summit flows, tephra, and caldera collapse. Bull. Volcanol. 66, 687–702.
Hay, R.L., Hildreth, W., Lambe, R.N., 1979. Globule ignimbrite of Mount Suswa, Kenya. In: Chapin, C.E., Elston, W.E. (Eds.), Ash-flow tuffs, Geological Society of America Special Publication, vol. 180, pp. 167–175.
Heiken, G., 1972. Morphology and petrography of volcanic ashes. Geol. Soc. Amer. Bull. 83, 1961–1988.
Heiken, G., 1974. An atlas of volcanic ash. Smithson. Contrib. Earth Sci. 12.
Heiken, G., 1978. Characteristics of tephra from Cinder Cone, Lassen Volcanic National Park, California. Bull. Volcanol. 41, 119–130.
Heiken, G., Lofgren, G., 1971. Terrestrial glass spheres. Geol. Soc. Amer. Bull. 82, 1045–1050.
Heiken, G., Wohletz, K., 1985. Volcanic Ash. University of California Press, Berkeley.
Hobbs, P.V., Radke, L.F., Stith, J.L., 1978. Response to "Particles in the eruption cloud from St. Augustine volcano" by Cadle and Mroz. Science 199, 457–458.
Houghton, B.F., Nairn, I.A., 1991. The 1971–1982 Strombolian and phreatomagmatic eruptions of White Island, New Zealand: eruptive and depositional mechanisms at a 'wet' volcano. Bull. Volcanol. 54, 25–59.
Houghton, B.F., Schmincke, H.-U., 1989. Rothenberg scoria cone, East Eifel: a complex Strombolian and phreatomagmatic volcano. Bull. Volcanol. 52, 28–48.
Hunt, J.B., Hill, P.G., 1993. Tephra geochemistry: a discussion of some persistent analytical problems. The Holocene 3, 271–278.
Huxley, L., 1918. Life and Letters of Sir Joseph Dalton Hooker O.M., G.C.S.I., Based on Materials Collected and Arranged by Lady Hooker, vol. 1. D. Appelton & Company, New York.
Jakobsson, S.P., Moore, J.G., 1986. Hydrothermal minerals and alteration rates at Surtsey volcano, Iceland. Geol. Soc. Amer. Bull. 97, 648–659.
Juvigné, É., Kozarski, S., Nowaczyk, B., 1995. The occurrence of Laacher See tephra in Pomerania, NW Poland. Boreas 24, 226–231.
Kelly, P.J., Dunbar, N.W., Kyle, P.R., McIntosh, W.C., 2008a. Refinement of the late Pleistocene to Holocene geologic history of Erebus volcano, Antarctica using $^{40}Ar/^{39}Ar$ and ^{36}Cl age determinations. J. Volcanol. Geotherm. Res. 177, 569–577 (this volume).
Kelly, P.J., Kyle, P.R., Dunbar, N.W., Sims, K.W., 2008b. Geochemistry and mineralogy of the phonolite lava lake, Erebus volcano, Antarctica: 1972–2004 and comparison with older lavas. J. Volcanol. Geotherm. Res. 177, 589–605 (this volume). doi:10.1016/j.jvolgeores.2007.11.025.
Keys, J.R., Anderton, P.W., Kyle, P.R., 1977. Tephra and debris layers in the Skelton Névé and Kempe Glacier, south Victoria Land, Antarctica. N.Z. J. Geol. Geophys. 20 (5), 971–1002.
King, E.A., Wagstaff, J., 1980. Search for cometary dust in the Antarctic ice. Antarc. J. U.S. 15, 78–79.
Kyle, P.R., 1977. Mineralogy and glass chemistry of recent volcanic ejecta from Mt. Erebus, Ross Island, Antarctica. N.Z. J. Geol. Geophys. 20, 1123–1146.
Kyle, P.R., Rankin, P.C., 1976. Rare earth element geochemistry of Late Cenozoic alkaline lavas of the McMurdo Volcanic Group, Antarctica. Geochim. Cosmochim. Acta 40, 1497–1507.
Kyle, P.R., Dibble, R.R., Giggenbach, W.F., Keys, J., 1982. Volcanic activity associated with the anorthoclase phonolite lava lake, Mt. Erebus, Antarctica. In: Craddock, C. (Ed.), Antarctic Geoscience. University of Wisconsin Press, Madison, pp. 735–745.

Kyle, P.R., Moore, J.A., Thirwall, M.F., 1992. Petrologic evolution of anorthoclase phonolite lavas at Mt. Erebus, Ross Island, Antarctica. J. Petrol. 33, 849–875.
Le Bas, M.J., Le Maitre, R.W., Streckeisen, A., Zanettin, B., 1986. A chemical classification of volcanic rocks based on the Total Alkali-Silica diagram. J. Petrol. 27, 745–750.
Lefèvre, R., Gaudichet, A., Billon-Galland, M.A., 1986. Silicate microspherules intercepted in the plume of Etna volcano. Nature 322, 817–820.
Lefèvre, R., Gaudichet, A., Leguern, F., 1991. Présence de microsphérules chimiquement variés dans les aérosols de certains fontaines de lave d'Hawaii. Comparaison avec l'Etna. C. R. Acad. Sci. Ser. 2 313, 105–111.
LeMasurier, W., Thompson, J., 1990. Volcanism of the Antarctic Plate and southern oceans. Antarctic Research Series, vol. 48. American Geophysical Union.
Lindstrom, D.J., Korotev, R.L., 1982. TEABAGS: computer program for instrumental neutron activation analysis. J. Radioanal. Chem. 70, 439–458.
Liu, H., 2000. Science and Engineering of Droplets, Fundamentals and Applications. William Andrew Publishing, LLC, Norwich.
Lyon, G.L., Giggenbach, W.F., 1974. Geothermal activity in Victoria Land, Antarctica. N.Z. J. Geol. Geophys. 17, 511–521.
Mangan, M.T., Cashman, K.V., 1996. The structure of basaltic scoria and reticulite and inferences for vesiculation, foam formation, and fragmentation in lava fountains. J. Volcanol. Geotherm. Res. 73, 1–18.
Marchant, D.R., Swisher III, C.C., Lux, D.R., West Jr., D.R., Denton, G.H., 1993. Pliocene paleoclimate and East Antarctic ice-sheet history from surficial ash deposits. Science 260, 667–670.
Marchant, D.R., Denton, G.H., Swisher III, C.C., Potter Jr., N.J., 1996. Late Cenozoic Antarctic paleoclimate reconstructed from volcanic ashes in the Dry Valleys region of southern Victoria Land. Geol. Soc. Amer. Bull. 108, 181–194.
Mastin, L.G., 1997. Evidence for water influx from a caldera lake during the explosive hydromagmatic eruption of 1790, Kilueau volcano, Hawaii. J. Geophys. Res. 102 (B9), 20,093–20,109.
Mastin, L.G., 2007. Generation of fine hydromagmatic ash by growth and disintegration of glassy rinds. J. Geophys. Res. B112 17 pp.
Meeker, G.P., Hinkley, T.K., 1993. The structure and composition of microspheres from the Kilauea volcano, Hawaii. Am. Mineral. 78, 873–876.
Moore, H.J., 1987. Preliminary estimates of rheological properties of the 1984 Mauna Loa lava. In: Decker, R.W., Wright, T.L., Stauffer, P.H. (Eds.), Hawaiian Volcanism. US Geol. Surv. Prof. Paper 1350, pp. 1569–1588.
Moore, J.A., Kyle, P.R., 1987. Volcanic geology of Mt. Erebus, Ross Island, Antarctica. Proceedings of the NIPR Symposium on Antarctic Geosciences vol. 1, Tokyo, Japan, pp. 48–65.
Moreno R., H., Fuentealba C., G., 1994. The May 17–19 1994 Llaima volcano eruption, southern Andes (38°42′S–71°44′W). Rev. Geol. Chile 21, 167–171.
Morrissey, M., Zimanowski, B., Wohletz, K., Buettner, R., 2000. Phreatomagmatic fragmentation. In: Sigurdsson, H., Houghton, B., McNutt, S.R., Rymer, H., Stix, J. (Eds.), Encyclopedia of Volcanoes. Academic Press, New York, pp. 431–445.
Moune, S., Faure, F., Gauthier, P.-J., Sims, K.W.W., 2007. Pele's hairs and tears: natural probe of volcanic plume. J. Volcanol. Geotherm. Res. 164, 244–253.
Naranjo S., J.A., Moreno R., H., Banks, N., 1993. La erupcíon del volcán Hudson en 1991 (46°S), Región XI, Aisén, Chile. Servicio Nacional de Geología y Minería, Chile, Boletin No. 44.
Ohba, T., Nakagawa, M., 2002. Minerals in volcanic ash 2: non-magmatic minerals. Glob. Environ. Res. 62 (2), 53–59.
Panter, K.S., Winter, B., 2008. Geology of the Side Crater of the Erebus volcano, Antarctica. J. Volcanol. Geotherm. Res. 177, 578–588 (this volume). doi:10.1016/j.jvolgeores.2008.04.019.
Perkins, M.E., Nash, W.P., Brown, F.H., Fleck, R.J., 1995. Fallout tuffs of Trapper Creek, Idaho—a record of Miocene explosive volcanism in the Snake River Plain volcanic province. Geol. Soc. Amer. Bull. 107, 1484–1506.
Perkins, M.E., Brown, F.H., Nash, W.P., McIntosh, W., Williams, S.K., 1998. Sequence, age, and source, of silicic fallout tuffs in middle to late Miocene basins of the northern Basin and Range province. Geol. Soc. Amer. Bull. 110, 344–360.
Rittmann, A., 1971. The Mt. Etna volcanic eruption of 1971. Smithsonian Inst. Center for Short-Lived Phenomena, 9 July.
Rolandi, G., Barrella, A.M., Borrelli, A., 1993. The 1631 eruption of Vesuvius. J. Volcanol. Geotherm. Res. 58, 183–201.
Rose, W.I., 1987. Active pyroclast processes studied with scanning electron microscopy. In: Marshall, J.R. (Ed.), Clastic Particles: Scanning Electron Microscopy and Shape Analysis of Sedimentary and Volcanic Clasts. Van Nostrand Reinhold Company, New York, pp. 136–158.
Rose, W.I., Hoffman, M.F., 1982. The May 18, 1980 eruption of Mount St. Helens: the nature of the eruption, with an atmospheric perspective. In: Deepak, A. (Ed.), Atmospheric Effects and Potential Climatic Impact of the 1980 Eruptions of Mount St. Helens, NASA Conference Publication 2240, pp. 1–14.
Ross, J.R., 1847. Voyage to the Southern Seas. John Murray, London.
Rowe, C.A., Aster, R.C., Kyle, P.R., Eschenbacher, A.E., 2005. Seismic observations at Mount Erebus Volcano Observatory: 1997–1998. Ant. J. US 33, 335–339.
Self, S., Sparks, R.S.J., 1978. Characteristics of widespread pyroclastic deposits formed by the interaction of silicic magma and water. Bull. Volcanol. 41, 196–212.
Self, S., Kienle, J., Huot, J.-P., 1980. Ukinrek Maars, Alaska, II. Deposits and formation of the 1977 craters. J. Volcanol. Geotherm. Res. 7, 39–65.
Shaw, H.R., 1972. Viscosities of magmatic silicate liquids: an empirical method of prediction. Am. J. Sci. 272, 870–893.
Shaw, H.R., Wright, T.L., Peck, D.L., Okamura, R., 1968. The viscosity of basaltic magma: an analysis of field measurements in Makaopuhi lava lake, Hawaii. Am. J. Sci. 266, 225–264.
Sheridan, M.F., Marshall, J.R., 1983. Interpretation of pyroclast surface features using SEM images. J. Volcanol. Geotherm. Res. 16, 153–159.
Simkin, T., Howard, K.A., 1970. Caldera collapse in the Galápagos Islands, 1968. Science 169, 429–437.
Sims, K., Blichert-Tofte, J., Kyle, P.R., Pichat, S., Gauthier, P.-J., Blusztajn, J., Kelly, P., Ball, L., Layne, G., 2008. A Sr, Nd, Hf, and Pb isotope perspective on the genesis and long-term evolution of alkaline magmas from Erebus volcano, Antarctica. J. Volcanol. Geotherm. Res. 177, 606–618 (this volume). doi:10.1016/j.jvolgeores.2007.08.006.
Smellie, J.L., 1999. The upper Cenozoic tephra record in the south polar region: a review. Glob. Planet. Change 21, 51–70.
Spadaro, F.R., Lefèvre, R.A., Ausset, P., 2002. Experimental rapid alteration of basaltic glass: implications for the origins of atmospheric particulates. Geology 30, 671–674.
Sun, S.S., Hanson, G.N., 1976. Rare earth element evidence for differentiation of McMurdo Volcanics, Ross Island, Antarctica. Cont. Min. Pet. 54, 139–155.
Sun, S.S., McDonough, W.F., 1989. Chemical and isotopic systematics of oceanic basalts: implications for mantle composition and processes. In: Saunders, A.D., Norry, M.J. (Eds.), Magmatism in Ocean Basins. Geological Society of London Special Publication, vol. 42, pp. 313–345.
Tallmadge, J.A., 1978. Powder production by gas and water atomization of liquid metals. In: Kuhn, H.A., Lawley, A. (Eds.), Powder Metallurgy Processing, New Techniques and Analyses. Academic Press, New York, pp. 1–32.
Thomas, R.M.E., Sparks, R.S.J., 1992. Cooling of tephra during fallout from eruption columns. Bull. Volcanol. 54, 542–553.
Thorarinsson, S., 1966. Surtsey: The New Island in the North Atlantic. Reykjavík, Almenna Bókafélagið.
van den Bogaard, P., Schmincke, H.-U., 1985. Laacher See tephra: a widespread isochronous late Quaternary tephra layer in central and northern Europe. Geol. Soc. Amer. Bull. 96, 1554–1571.
Walker, G.P.L., Croasdale, R., 1971. Characteristics of some basaltic pyroclasts. Bull. Volcanol. 35, 305–317.
Wohletz, K.H., 1983. Mechanisms of hydrovolcanic pyroclast formation: grain-size, scanning electron microscopy, and experimental studies. J. Volcanol. Geotherm. Res. 17, 31–63.
Wohletz, K.H., McQueen, R.G., 1984. Volcanic and stratospheric dustlike particles produced by experimental water-melt interactions. Geology 12, 591–594.
Yule, A.J., Dunkley, J.J., 1994. Atomization of melts for powder production and spray deposition. Oxford Series on Advanced Manufacturing, vol. 11. Clarendon Press, Oxford.
Zimanowski, B., Lorenz, V., Frohlich, G., 1986. Experiments on phreatomagmatic explosions with silicate and carbonatitic melts. J. Volcanol. Geotherm. Res. 30, 149–153.
Zimanowski, B., Büttner, R., Lorenz, V., Häfele, H.-G., 1997. Fragmentation of basaltic melt in the course of explosive volcanism. J. Geophys. Res. 102, 803–814.